UNIVERSIDAD
NACIONAL
DE COLOMBIA

Improvement of Digital Lensless Holographic Microscopy for the visualization of biosamples

Samuel Ignacio Zapata Valencia, Eng

Universidad Nacional de Colombia
Facultad de Ciencias, Escuela de Física
Medellín, Colombia
2023

Improvement of Digital Lensless Holographic Microscopy for the visualization of biosamples

Mejoramiento en la visualización de muestras biológicas en microscopía holográfica digital sin lentes.

Samuel Ignacio Zapata Valencia, Eng

Thesis presented as a partial requirement qualify for the title of:
Magister en Ingeniería Física

Advisor:
Jorge Iván García Sucerquia, Ph.D.

Research field:
Digital Holographic Microscopy

Research group:
Optics and Opto-digital Processing

Universidad Nacional de Colombia
Facultad de Ciencias, Escuela de Física
Medellín, Colombia
2023

Each time you try, gonna get just a little bit better
Each step you climb is one more step up the ladder

Agradecimientos

En esta sección quiero expresar mis agradecimientos a aquellas personas que compartieron su tiempo, apoyaron el desarrollo de esta maestría. Gracias por alivianar este proceso.

Agradezco al profesor Jorge Iván García Sucerquia, por su orientación en el desarrollo de este trabajo y sobre todo en mi formación profesional. Por ayudarme a construir cimientos sólidos, sobre los cuales podré empezar a construir nuevos caminos. Por enseñarme a trabajar entendiendo muy bien lo que estoy haciendo, y para qué lo estoy haciendo. Por siempre apoyarme sin dudar en esas ideas raras que se me ocurrieron. Por regañarme y motivarme a ser un poco más rebelde. A él, por hacer muchísimo más que solo su trabajo.

A los demás integrantes del Grupo de Óptica y Procesamiento Optodigital. A Heber, por siempre encontrar la manera de sacar lo mejor de mí, por esas discusiones de horas para ponernos de acuerdo, por acompañarme en este camino, lo empezamos juntos y vamos por más; más risas y lágrimas, más reuniones de medianoche, más viajes y congresos, más microscopía y óptica. A Carlos, por traerme a este hermoso mundo de la holografía, por esas largas conversaciones, por enseñarme y permitirme enseñar, por escuchar mis crisis y ayudarme a apaciguarlas, porque en él encontré otro tutor y un gran amigo. Y a Aleja por siempre estar pendiente, por mostrarme que hay tiempo para todo. A los tres por acompañarme durante esas largas horas en el laboratorio, y hacer que el paso del tiempo no se sintiera.

A Pablo, Rafael, Ana, Francisco, y los demás miembros del Capítulo Estudiantil de Óptica. Por permitirme divulgar ciencia junto a ustedes, de crecer juntos y orientar a las nuevas generaciones a continuar con esta bella labor.

A Pipe, Brayan y los miembros del Laboratorio de Diseño Mecánico, por siempre estar disponibles y permitirme utilizar el taller con el fin de avanzar con el desarrollo de esta tesis.

Aprovecho para agradecer enormemente a los profesores Yamile Cardona y Juan Fernando Botero, porque fueron ellos los que sin dudar me abrieron las puertas en el mundo de la óptica.

Al profesor Román Castañeda. Gracias a él, en la portada de esta tesis dice «Ingeniería».

A la profesora María Sagrario Millán (Universitat Politècnica de Catalunya), por su gran apoyo en mi desarrollo profesional.

A SPIE y Photonics Media por otorgarme la beca Teddi C. Laurin. A OPTICA por otorgarme. Por promover de diferentes formas mi desarrollo profesional en el área de la óptica.

A Diego, Julián, Abraham, Juan Pablo, Juanes, Víctor, por los momentos de distracción que compartimos y la colaboración que en uno u otro momento me prestaron.

A la profe Liliana, Wilson, Santiago, Laura, Daniel, David, por ayudarme a colocarle un poco de música a este camino.

A Valen, Simón, Camila y al resto de mi familia por el apoyo que me brindaron para seguir adelante con este proyecto. Quiero destacar especialmente a Valen, por su incondicional apoyo en todo lo que necesité.

A mi hermanita, por acompañarme día a día en este camino, por aguantar todos mis dramas, por todos los secretos y sueños, por crecer conmigo. A mi gato Gardel, por acompañarme durante noches enteras, y largas horas de trabajo, porque ambos tuvimos mucha suerte al encontrarnos.

A mi mamá y a mi papá por su apoyo incondicional, por no dudar un segundo de mí, por preocuparse si estaba bien, porque siempre estuvieron ahí. Sin ustedes nada de esto hubiera sido posible. Los amo.

A todos ustedes y a los que pasé por alto, muchas gracias.

Resumen

La Microscopía Holográfica Digital sin Lentes (DLHM) es una técnica de imagen que ha sido utilizada para la visualización de muestras de tamaño micrométrico. La simplicidad en el hardware requerido, la adaptabilidad en el procesamiento digital y la no necesidad de marcadores la han posicionado como una alternativa atractiva, portable y eficiente en términos de costos para la visualización de muestras biológicas micrométricas. A pesar de la simplicidad en su implementación, los componentes de hardware utilizados para capturar los hologramas digitales tienen limitaciones que afectan directamente la correcta visualización de muestras.

En la presente tesis de maestría en Ingeniería Física, se estudian las limitaciones en el hardware de DLHM y su impacto para la visualización de objetos microscópicos. A su vez, se proponen mejoras a estas limitaciones por medio de la implementación de métodos opto-numéricos los cuales son validados por la visualización de muestras biológicas. Dada la importancia de la apertura numérica (NA) para el rendimiento en DLHM, se presenta un método para la caracterización y validación de la NA en haces de luz. Se propone además un método para la expansión del campo de visión de los objetos observados. Finalmente, se propone un método para corregir los hologramas en línea de DLHM con el fin de eliminar artefactos inherentes a la fuente de iluminación y también para recuperar la información de objetos con estructura visualizados en DLHM.

Además de esto, adjuntos con esta tesis se encuentran dos manuscritos publicados en revistas indexadas de circulación internacional y 5 resúmenes aprobados o actas de congresos internacionales, donde los resultados de esta tesis fueron presentados.

Palabras clave: microscopía holográfica digital sin lentes, limitaciones de DLHM, apertura numérica, campo de visión, artefactos en la iluminación, oclusiones.

Abstract

Digital Lensless Holographic Microscopy (DLHM) is an imaging technique that has been used to visualize micrometer-sized samples. The simplicity of the required hardware, the adaptability of digital processing, and its label-free attribute have positioned it as an attractive, portable, and cost-effective alternative for observing microscopic biological samples. Despite the simplicity of its implementation, the hardware used to record the digital holograms has limitations that directly affect the visualization of biological samples.

In this master's thesis in Engineering Physics, the identified limitations of the DLHM hardware and their impact on the visualization of micrometer-sized objects are studied. An improvement of those limitations is proposed by implementing opto-numerical methods, which are tested by visualizing biosamples. Given the importance of the Numerical Aperture (NA) for the performance of DLHM, a method for characterizing and validating the NA of propagating beam illuminations is developed. A method for expanding the field of view of the visualized samples is presented. Finally, a multiview method for correcting DLHM in-line holograms is proposed to eliminate illumination artifacts inherited from the illumination source, and also to recover the information of occluded structured samples visualized in DLHM.

The results were reported on two manuscripts already published in indexed journals of international circulations and five proceedings or submitted abstracts of presentations at international conferences.

Keywords: digital lensless holographic microscopy, DLHM limitations, numerical aperture, field of view, illumination artifacts, occlusions.

Content

List of figures

Introduction

Digital Lensless Holographic Microscopy (DLHM) is a two stages imaging technology of interest for the label-free visualization of micrometer-sized samples with a high performance and low cost [1,2]. A point source of spherical waves and a digital camera are the needed hardware to work. In the recording stage, the spherical wavefront illuminates the sample and produces a diffraction pattern whose intensity, known as hologram, is recorded in the digital camera [1]. In the reconstruction stage, the complex-valued wavefield scattered by the sample is numerically retrieved by computing the backwards propagation of the digital hologram [3]. This is achieved through numerical scalar diffraction methods [3–5]. From the retrieved wavefield, either the intensity or phase information of the sample can then be computed [6].The simplicity of the required hardware and the versatility of digital processing the recorded holograms make DLHM an attractive alternative for visualizing microscopic biological samples [7]. Additionally, being an holographic technique, it allows the label-free visualization of specimens that typically require staining due to their lack of color and contrast [8]. This makes possible the observation of micrometer-sized specimens like cells or microorganisms [9], without employing staining agents that could chemically react with the specimens and potentially cause harm [8].

The simplicity of the required hardware, the adaptability of digital processing and the its label-free feature make DLHM an attractive tool for visualizing microscopic biological samples [7]. However, due to this same simplicity, the optical properties of the few hardware components strongly determine the final image quality. This gives rise to several limitations that can constrain the adoption of this technology. For the study of biological samples, the accurate characterization of the numerical aperture of the point source, the reduced field of view (FOV) when a large magnification is required to the accurate sampling of higher frequencies diffracted by the specimens, the possible presence of noise artifacts in the illumination profile, and the occlusion of objects in the same line of sight of a volumetric sample, are particularly troubling.

The performance of the technique strongly depends on the Numerical Aperture (NA) of the illumination source [1]. The larger the value of the NA, the better the achievable resolution. The traditional implementation of DLHM uses a pinhole-based illumination source; nevertheless, multiple alternatives sources have been explored for their use in DLHM. Commercial optical elements, such as aspherical [2,10,11] and diffractive-refractive lenses [12], have been utilized to generate the needed spherical wavefront. For these elements, the graded NA value reported by the manufacturer should be validated. Moreover, manufacturing custom illumination sources, such as optical fiber cone tips [13–15] and holographic point sources [16], have been adapted to the DLHM setup. For these sources, a characterization is required, as there is not a graded NA value available. Consequently, a technique for the characterization and validation of the NA of propagating light beams was developed, implemented, and tested.

DLHM presents improvement opportunities for its uses in biological applications. For the visualization of smeared micrometer-sized biosamples, such as red blood or epithelial cells [9], a large field of view (FOV) is often required to include enough amount of cells in the visualized image. In DLHM, increasing the FOV area results in a decrease in the magnification of the diffraction pattern of the sample. This reduction may jeopardize the correct sampling of the diffracted information in the recorded hologram. To prevent this problem, it is necessary to develop methodologies for expanding the FOV while maintaining a properly sampling the diffracted information. There is one reported method for expanding the FOV in DLHM [17]; however, its implementation requires including additional hardware elements in the point source setup, spoiling the simplicity of the conventional setup. A solution that can increase the FOV for DLHM without affecting the simplicity of the conventional setup was sought and developed.

The above considerations assume that the wavefront emerging from the point source is an ideal spherical wave. Thus, as an ideal spherical wave does not exist, the wavefronts produced by the alternative illumination sources could carry illumination artifacts. As the quality of the spherical wavefront directly affects the recovered sample information [18], the presence of any artifact inherited from the illumination source produces a ruined visualization of the sample in the region where the artifact is located. Moreover, for the application in biosamples visualization, those artifacts lead to deteriorated visualization of the specimen, which may conceal the identification of the structure of the sample. The current approach to tackle this problem includes the numerical calculation of a contrast hologram for eliminating imperfections in the illumination source [1,19], the application of filtering techniques typical to imaging processing for decreasing the impact of the illumination artifacts [20,21], and hologram normalization alternatives for solving the illumination inhomogeneities [18,22]. Despite their effectiveness to alleviate light inhomogeneities of the wavefront, they failed when applied to remove massive and strong illumination artifacts. Hence, a method to remove the presence of illumination artifacts that can distort the displayed images in DLHM was developed.

The visualization of biosamples can be extended to volume samples, such as swimming specimens [14,23], even in wild environments [24]. For this application, DLHM is an attractive technique, given that the in-line hologram records the information from the whole illuminated volume; this allows the possibility of a-posterior focusing of the specimens at different axial positions of the volume. In that way, it is possible to record the diffraction pattern of occluded samples, namely when more than one specimen is in the same line of sight in the visualized volume [25], producing a recorded hologram with superimposed information of the samples. Consequently, as the digital hologram carries all the recorded information scattered by the specimens in the volume, the numerical reconstruction for occluded specimens carries a distortion in the imaged sample, affecting the quality in the visualized specimens. An occlusion removal method is required in DLHM, given that no methods are reported to date. Hence, an occlusion removal method was developed, implemented, and tested in DLHM recordings.

Finally, access to microscopy equipment is commonly limited to well-funded laboratories, given the high cost of the optical components, such as microscope objectives and lenses. The simplicity of the hardware previously presented for DLHM reports an opportunity to develop cost-effective prototypes in which the reduced hardware components imply a reduced price. In this way, the Optics and Opto-Digital Processing Research Group developed the most cost-effective microscope with the DLHM technology reported to date, costing approximately US$53.00 [2]. The surveillance digital camera utilized for the hologram recording in that microscope is the most expensive element, costing approximately US$43.40. Adapting lower-cost commercial digital cameras could reduce the cost of the device, but the optical characteristics of low-cost sensors could reduce the optical performance of the technique. Using the previously presented approaches, these limitations are surpassed, showing that even budget cameras can be used to achieve research-grade imaging in DLHM architectures.

All the above-mentioned approaches allow the alleviation of the identified limitations for the DLHM adoption in the observation of biosamples. In this master's thesis in Engineering Physics, the development of these methods and their application in visualization of biosamples are presented. Chapter 1 introduces the conceptual background and state-of-the-art for the content of the next chapters. Chapter 2 presents the development of the Multiview Correlation Method for correcting in-line holograms in DLHM. Chapter 3 presents a technique for characterizing and validating the NA of propagating Gaussian beams. Furthermore, a method is presented for expanding the FOV in DLHM. These advancements have been integrated into a cost-effective microscope, enhancing its capabilities with a further reduction in cost. Chapter 4 presents the application of the Multiview Correlation Method for correcting artifacts inherited from the illumination source. Chapter 5 presents the recovery of the information from samples in the presence of occlusions by applying the Multiview Correlation Method. Finally, Chapter 6 concludes with the main results achieved, and the perspectives of future work that can be derived from them.

The most significant novel results that have been derived from this master's thesis have been reported in papers published in indexed journals of international circulation such as:

- "*Automatic method to measure the numerical aperture of a propagating Gaussian light beam*", Óptica Pura y Aplicada **55**, 1-8 (2022) [26].
- "*Image enhancement and field of view enlargement in digital lensless holographic microscopy by multi-shot imaging*," J. Opt. Soc. Am. **A 40**, C150-C156 (2023) [27].

Additionally, the most significant results were presented in scientific conferences of international scope in the form of both oral and poster presentations as follows:

- "*Método automático para la medición de la apertura numérica de haces de luz Gaussianos"*, XVII Encuentro nacional de Óptica y XIII Conferencia Andina y del Caribe en Óptica y sus aplicaciones, Medellín Colombia, 2021 [28].
- *"Cost-effective digital lensless holographic microscope,"* in OSA Imaging and Applied Optics Congress (Online), Washington DC United States, 2021 [29].

- *“Improvement of the image reconstruction in digital lensless holographic microscopy by scanning of the sample plane,"* in Latin America Optics and Photonics (LAOP) Conference 2022, Technical Digest Series (Optica Publishing Group, 2022), paper W1D.2. [30].
- *“Removal of perturbations from Optical-Pickup-Unit-based illumination for Digital Lensless Holographic Microscopy”*, XI Iberoamerican Optics Meeting / XIV Latin American Meeting on Optics, Lasers and Applications (RIAO-OPTILAS), San José, Costa Rica, 2023 [31]. Awarded with the **Third Place in Poster presentation.**
- *“Recovery of occluded objects in digital lensless holographic microscopy”*, XI Iberoamerican Optics Meeting / XIV Latin American Meeting on Optics, Lasers and Applications (RIAO-OPTILAS), San José, Costa Rica, 2023 [32].

1. Digital Lensless Holographic Microscopy

1.1 Fundamentals of Digital Lensless Holographic Microscopy

The original conception of Digital Lensless Holographic Microscopy (DLHM) was proposed by Dennis Gabor in 1948 [33]. In that work, a two-step imaging method for the visualization of micro-sized objects was introduced. The core of this invention was the achieving of a lens-free magnified image of the sample by the free space propagation of the diffraction pattern of the sample, as it was illuminated by a divergent wavefront of electrons. In the first step of this technique, a divergent spherical wavefront $\exp(ikr_0)/|r_0|$ illuminates a weak scattering sample $S(\vec{r}_0)$ located at a distance z close to the point source that produces the said wavefront. The diffracted wavefield,

$$U(\vec{r}) = \int_{Sample} S(\vec{r}_0) \frac{\exp[ik\vec{r}_0]}{|\vec{r}_0|} \frac{\exp[ik(\vec{r} - \vec{r}_0)]}{|\vec{r} - \vec{r}_0|} d\vec{r}_0 \tag{1.1}$$

carrying the information of the sample, propagates towards a photographic plate located at a distance L from the said source, as shown in Fig. 1-1. The position vectors $\vec{r}_0(x_0, y_0, z)$ and $\vec{r}(x, y, L)$ denote a sample plane and the photographic plate plane, respectively, measured from the point source. There, the recorded intensity $I(\vec{r}) = U(\vec{r})U^*(\vec{r})$ is known as a hologram [34].

For the second step, the hologram recorded on the photographic plate is directly illuminated by an illumination wavefront, without the presence of the sample. As the complex-valued wavefield of the sample is coded in the holographic plate, an image of the sample can be visualized in a position and with magnification dictated by the holographic equations [35].

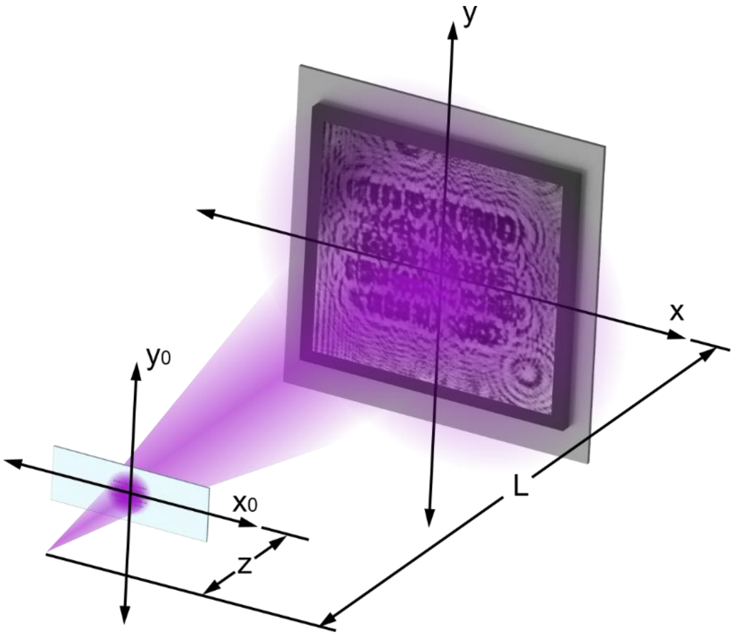

Fig. 1-1. Illustration of DLHM architecture

The development of new technologies enhanced both stages of Gabor proposal, what led to it is known as DLHM [1]. For the recording stage, the electrons source has been replaced by a point source emitting visible light and the photographic plate has been replaced by a digital sensor; the latter helps to overcome the laborious wet chemical processes for the recording of the hologram [36] and enables the articulation of the versatility and opportunities of the digital world in the process of the sample information recovery for the reconstruction stage. The use of digital cameras in DLHM allows easily multiple recordings during the recording stage, such as the reference $I_{Ref}(\vec{r})$ wavefront, which corresponds to the intensity produced by the point source without the presence of the sample.

The second step of Gabor proposal's has been replaced by a numerical processing of the digital recorded hologram [36]. A pixel-wise subtraction of the reference from the recorded hologram is calculated as:

$$\tilde{I}(\vec{r}) = I(\vec{r}) - I_{Ref}(\vec{r}). \tag{1.2}$$

This information is known as contrast hologram [1,19] and is aimed to remove the presence of the zero-diffraction order from the recorded information of the sample [37]. The computation of the numerical diffraction that a converging spherical wavefront $exp[-ik\vec{r}]/|\vec{r}|$ undergoes as it illuminates the contrast hologram [3,4]:

$$U(\vec{r}_0) = \int_{\substack{Digital\\camera}} \tilde{I}(\vec{r}) \frac{\exp[-ik\vec{r}]}{|\vec{r}|} \frac{\exp[-ik(\vec{r}-\vec{r}_0)]}{|\vec{r}-\vec{r}_0|} d\vec{r} \qquad (1.3)$$

allows the recovery of the complex-valued information of the sample at its corresponding imaging plane. From this complex wave-field, the amplitude $A(\vec{r}_0) = |U(\vec{r}_0)|$, the intensity $I(\vec{r}_0) = |U(\vec{r}_0)|^2$ and the phase $\phi(\vec{r}_0) = \mathrm{atan}\{\mathrm{Im}[U(\vec{r}_0)]/\mathrm{Re}[U(\vec{r}_0)]\}$ can be computed, with $\mathrm{Re}(\ \ )$ and $\mathrm{Im}(\ \ )$ being the real and imaginary components of the complex field, respectively, and the function $\mathrm{atan}(\ \ )$ being the arc-tangent function.

1.1.1 Multiplexing in DLHM

The simplicity in the process of recording a digital hologram in DLHM and the linearity in amplitude of the recorded holograms [6], allow the possibility of using the superposition principle to easily record and consequently add digital holograms without losing information about the imaged samples. This fact has been explored in time multiplexing for trajectory particle tracking [19]. A stack of time-spacing N digital holograms I_n is recorded; in the first approach for trajectory particle tracking, each hologram of the stack can be reconstructed, and the movement of the scene can be observed by individual reconstruction of each hologram of the stack. This process can be simplified by utilizing the superposition principle of DLHM. Initially, by adding the contrast holograms of the time-spacing stack of holograms, a new one with the information in time of the same object can be obtained. This enables the reconstruction of just one hologram, where the displacement of the sample can be observed. Then to improve the performance, the contrast hologram is not calculated for each recording of the stack. In a better approach, consecutive hologram pairs are pixel-wise subtracted to eliminate the nuisance of the converging illumination wave, and the result is added to compose the time-tracking hologram $I_{Track}(x,y)$ as

$$I_{Track}(x,y) = \frac{1}{N/2} \sum_{i=1}^{N/2} I_{2i-1}(x,y) - I_{2i}(x,y)\,. \qquad (1.4)$$

Finally, equation(1.3) is computed for $I_{Track}(x,y)$ to recover the complex-valued wavefield of all the information of the displaced sample in one recovered scene. Fig. 1-2 shows the application of this method for the visualization of a Rotifer swimming at a speed of 2.5mm/s recorded by a submersible microscope at a depth of 15 m in the North Atlantic [6,23].

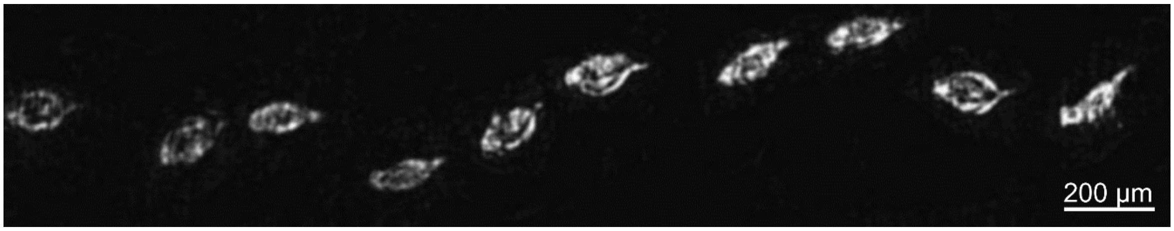

Fig. 1-2. Timing visualization of a swimming Rotifer [6,23].

1.2 Limitations in the visualization of biosamples

The visualization of biological micrometer-sized samples has been a challenge in research. The transparent characteristic of biological specimens generates that the use of imaging techniques such as brightfield microscopy, requires the utilization of stains in the samples for a correct visualization of the sample [8]. On the other hand, holographic techniques such as DLHM do not require the use of labels or staining to visualize microscopic images [7]. In these techniques, the recorded hologram codes the amplitude and phase information of the sample, and by computing a numerical reconstruction process, the complex-valued wavefield scattered by the sample can be recovered. This approach minimizes the interaction with the sample and allows the study of biological samples without the chemical intervention and possible poisoning effects of labels [8].

The visualization of smears samples, such as red blood or epithelial cells, is common in biological studies [9,38]. For visualizing those smears samples, a large field of view (FOV) is required to observe more cells quantity in the same image. In DLHM, the larger the FOV, the less the magnification of the diffraction pattern of the imaged sample, which may ruin the correct sampling of the specimen information in the recorded hologram; consequently, affecting the recovering of the information of the scattered wave-field. The presence of inhomogeneities or artifacts in the illumination leads to altered visualization of the specimens after their reconstruction. When imaging biosamples, these alterations may conceal critical details for the identification of the structure of the sample, thus limiting the usability of the technique. Moreover, the visualization of sample volume could be affected by occlusion presence. For DLHM, while the digital hologram carries all the recorded information scattered by the specimens in the volume, the presence of multiple specimens in the same line of sight generally hinders the correct visualization of the samples in the reconstruction.

The capabilities of DLHM for visualizing biological samples have been studied in different specimens, including millimeter-sized such as *Drosophila melanogaster* fly [39], and starch grains [40], as well as micrometer-sized organisms such as algae [19], protozoa [23], bacteria [41], and cells such as epithelial human cells [2], and red blood cells [2,13].

Similarly to the case of conventional optics methods, different implementations have been incorporated into the DLHM conventional setup to improve the capabilities of the technique, including multi-wavelength coherent illumination for color imaging [39], the addition of polarizers to analyze anisotropy of biological samples [40], the utilization of an electrically tunable lens to provide variable zoom to the technique [42]. While some of these implementations require hardware modifications, others are purely computational and maintain the simplicity of the DLHM hardware, such as recording holograms of successive positions of microorganisms for trajectory tracking [19,23,43] and normalization algorithms for improving the contrast in the reconstruction [18]. Limiting the hardware to only two components has made possible the development of compact microscopes for biological sample visualization [2,10,13,23,24,41]. Although the simplicity of the hardware components is a benefit for the implementation of the technique, it also means that the optical properties of these components strongly influence the quality of the imaged samples. The next subsections will examine the challenges and limitations of the conventional hardware used in DLHM, including the digital sensor, the point source illumination, and the sample, in terms of their impact in the recording process of the digital holograms.

1.2.1 Numerical Aperture and FOV

The performance of DLHM in terms of the spatial resolution is governed by the numerical aperture (NA) of the microscope [1,33]. Accordingly, a DLHM microscope can distinguish two object points that are separated by a lateral distance Δr if

$$\Delta r \geq \frac{\lambda}{2\,NA}, \tag{1.5}$$

and by an axial distance Δz if:

$$\Delta z \geq \frac{\lambda}{NA^2} \;, \tag{1.6}$$

with λ the wavelength of the illumination source. In DLHM, the NA is determined by the smallest value between the NA of the illuminating point source as

$$NA = n\sin\theta \;, \tag{1.7}$$

where θ is the half-angle of the cone light and n is the refractive index of the medium [44], and the NA defined by the geometry of the recording setup as

$$NA = \frac{W}{2\sqrt{\left(\frac{W}{2}\right)^2 + L^2}} \;, \tag{1.8}$$

where W is the width of the recording sensor.

For DLHM exists an effective architecture when the NA of the illumination is equal to the geometric NA; in this configuration, the light source fully illuminates the digital sensor. The characterization of the light source in terms of the NA and the size of the sensor W, determine the effective value of L distance by simple geometry. When a smaller L distance is used, the digital sensor is not fully illuminated by the light source, resulting in non-used zones in the sensor. On the other hand, when a larger L distance is used, the clipping of the illumination by the effective sensing area, leads to a loss in the achievable resolution of the technique, as shown in equations (1.5) and (1.6). Knowing the illumination NA and W values of the utilized microscope, is essential to determining the best architecture for providing the best performance to DLHM.

The NA depends only on the illumination source and only affects the propagation of the sample information towards the recording plane. However, W depends on commercial digital sensors, and their specifications constraint the recorded information on the digital hologram. These limitations in terms of the recording system have been determined by analyzing the hologram recording of two-point scatters separated by a distance t [23], as is shown in Fig. 1-3. Both point scatters were located at a z distance from the point source, and the diffraction pattern was produced over the digital sensor plane at a distance L from the said source. The digital camera records the interference of the diffraction pattern of both independent point scatters illuminated by the spherical wave [45]. This interference produces a modulation depending on the separation t between both scatters [23]. Given the finite size of the digital sensor, a requirement where at least the first enveloped modulation is recorded on the sensor was proposed, and the limits for the separation t between two-point scatters were determined for DLHM. A geometric analysis for the setup provide an expression for the sensor size as [23]:

$$W = \frac{(L - z)\lambda}{\sqrt{t^2 - \left(\frac{\lambda}{2}\right)^2}}. \tag{1.9}$$

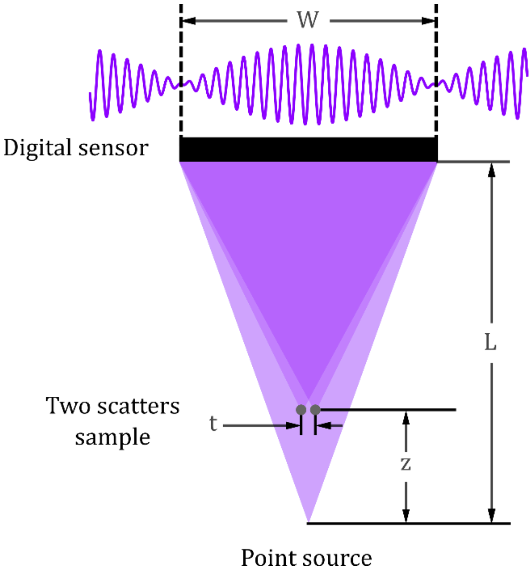

Fig. 1-3. Hologram recording of two-point scatters in DLHM architecture.

In this expression, the smaller the t distance between the scatters, the larger the size of the sensor, and when that distance is half of the used wavelength, a sensor of infinity length is needed to record at least the first enveloped modulation pulse. Indeed, does not exist a commercial sensor of that length, but that value indicates that a large size of the sensor is crucial for properly recording the digital in-line holograms. In the same line of the sensor, to guarantee a correct sampling of the diffraction pattern of the sample, according to [23], the smaller fringe spacing diffracted by the sample over the sensor plane should be recorded at least by 3 pixels, determining in this way the pixel size as

$$\Delta p < \frac{L-z}{3\sqrt{\frac{1}{NA^2}-1}} \tag{1.10}$$

Finally, the geometric parameters L and W of the architecture of DLHM or the used NA, in conjunction with the source to sample distance z, determine the FOV as
Finally, the FOV of the DLHM architecture can be defined in two ways, first in terms of the geometric parameters L and W, and second, in terms of NA; both definitions depend on the source to sample distance z, as

$$FOV = \begin{cases} \left(\frac{Wz}{L}\right)^2 \\ \frac{(2NAz)^2}{(1-NA^2)} \end{cases} \tag{1.11}$$

for a square sensor of W side. Consequently, the magnification M of the diffraction pattern of the object over the digital sensor is defined as

$$M = \frac{L}{z} \tag{1.12}$$

To summarize, the maximum performance of DLHM architecture is limited by three parameters: NA of the illumination, W size of the digital sensor, and pixel size. These parameters directly impact on the achievable resolution of the technique, and the first two parameters define the FOV of the visualized samples.

1.2.2 Illumination artifacts

In DLHM, as the magnification of the recorded digital hologram is produced by the free-space propagation of the diffraction pattern of the sample as it is illuminated by a diverging wave, the quality of the recovered image depends strongly on the quality of the recorded illuminating wavefront; the closer the illumination to a perfectly clean spherical wavefront as shown in Fig. 1-4 (a), the better the quality of the reconstructed image [18]. Any inherent inhomogeneity in the illuminating wavefront is carried towards the digital sensor and is scrambled in the recording of the sample information.

Additionally, according to equations (1.5) and (1.6), the best performance of DLHM in terms of spatial resolution is achieved using the larger possible NA illumination source. The most common method for generating a spherical wave illumination in DLHM is focusing the light of a laser onto the surface of a metallic pinhole with a diameter close to the illumination wavelength. Despite the effectiveness in terms of reaching NA values close to 0.77 [1], the need for very precise and robust optomechanical devices turns this method very unstable, resulting in non-symmetrical distorted illuminating wavefronts [14]; interference ring-like artifacts are also commonly presented due to reflections produced in the sensors protective glass layers and infrared filters, which are widely added to the digital recording systems, as seen in Fig. 1-4 (b). All the previously mentioned inhomogeneities are inherited in the recovered image, decreasing the performance and quality of the final reconstructed images in DLHM. In Fig. 1-4 (c), the inherited ring-like structures produced in a pinhole DLHM approach in the reconstruction of the tip of an acupuncture needle are shown. Additionally, small tilts in the alignment of the microscope could lead to reflective artifacts between the pinhole metallic surface and the sample slide, as seen in Fig. 1-4, panel (d), where a 100 µm circle from a calibration microscopy slide is imaged. It is of great concern that these reflective artifacts become larger when the microscope slide is closer to the illumination source, because this is the common setup in DLHM for the proper magnification of the sample information pattern.

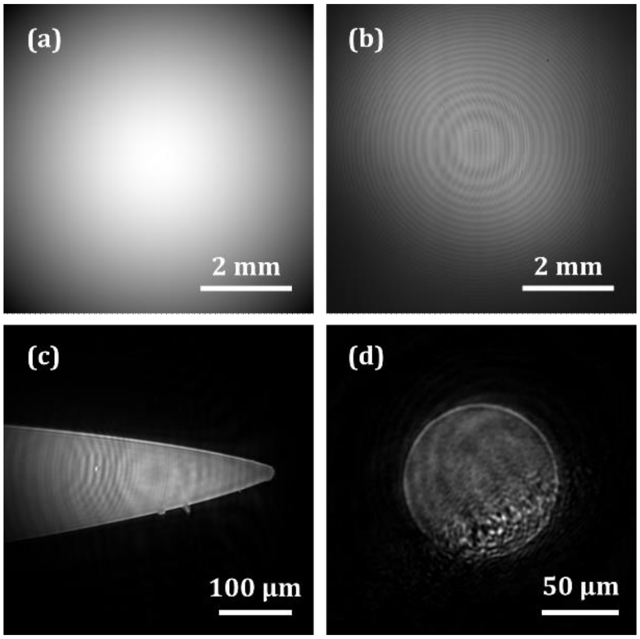

Fig. 1-4. DLHM point source and intensity reconstructions. Panel (a) shows a numerical generated point source of spherical waves. Panel (b) shows a 1 µm pinhole illumination, panel (c) shows the reconstruction of the tip of an acupuncture needle, panel (d) shows the intensity reconstruction of a 100 µm circle from a calibration microscopy slide.

Options for the pinhole approach have already been reported. Graded-index lenses [41] and holographic point sources [16] have also been used in lensless imaging systems to produce the needed illuminating spherical wavefront; in somehow a similar way to the pinhole-based technique, those methods require the use of robust optomechanical components for the precise alignment of the system. Engineered optical fibers have been utilized to produce point sources with NA of 0.88 [13–15]. However, this approach has the disadvantage that this optical fiber exhibits a high sensitivity to dust and mechanical fragility.

Aspherical and refractive-diffractive lenses are some of the best current options to produce the needed spherical wavefronts in DLHM [2,10,11,46,47]. The former can produce neat spherical wavefronts at a limited range of NA and has been utilized in DLHM to produce the most cost-effective label-free microscope reported to date [16] using an aspherical lens of $NA = 0.67$. Moreover, the refractive-diffractive lenses produces spherical wavefronts at NA above 0.85, as the Optical Pick-up Unit (OPU) diffractive lens [48,49], but presents massive ring-like structure artifacts as shown in panel (a) of Fig. 1-5, produced by the edges of the phase shift diffractive structures, which are persistent in the imaged samples as inherited artifacts at the same time that limits the usable FOV for the sample imaging [12]. Nevertheless, both types of lenses demand a collimated illumination source and are easily dusted as they are out of a controlled lab environment Fig. 1-5 (b).

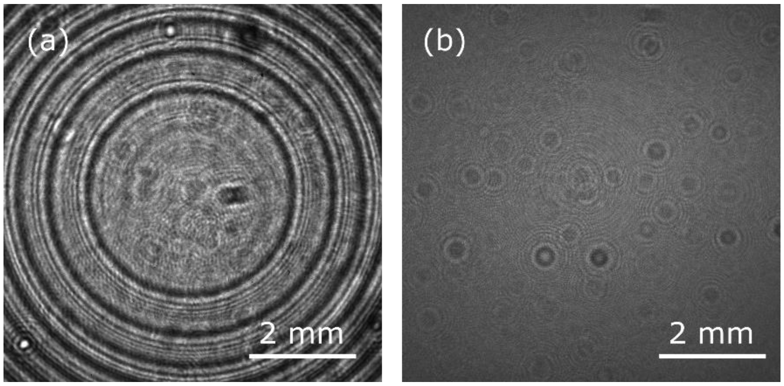

Fig. 1-5. Recorded illumination in DLHM without the interest sample. Panel (a) shows the illumination produced by a Blu-ray OPU focusing lens. Panel (b) shows the dusted illumination of an aspherical lens out of controlled environmental conditions.

Different strategies have been proposed to overcome the effects of those illumination artifacts over the reconstructed image. The first and simplest is the reconstruction of the contrast hologram [19] presented in equation (1.2); the subtraction of the recorded reference eliminates inhomogeneities of the illumination, but it does not work properly for all of the cases and does not solve the artifacts presence. Additionally, different standard filtering techniques have been applied to the contrast hologram, such as median, Non-Local Mean (NLM) [20], and Block-matching and 3D (BM3D) filters [21], to decrease the presence of illumination artifacts; but similar to the contrast hologram, does not fully overcome the influence of illumination artifacts and in some cases could result in a resolution reduction. Finally, methods for normalizing the DLHM holograms and correcting the effects of the illumination inhomogeneities, such as Barton's method [22] and its modification [18], have also been used in DLHM. These methods enhance the contrast of the reconstructions but do not fully solve the artifacts problem.

To illustrate the incidence of illumination artifacts over the recovered images in DLHM, an USAF test target [50] was imaged utilizing a DLHM microscope based on a OPU as illumination source, with NA of 0.85. The presence of the ring-like structures artifacts, product of the diffractive-refractive structure of the outer lens of the OPU, is evident in the recorded hologram as is shown in Fig. 1-6 (a). Despite the theoretical high spatial resolution this *NA* could produce, the inhomogeneities perturb the reconstruction of the contrast hologram, leading to a poor-quality resulting image, destroying the sample information as shown in panel (b) of Fig. 1-6.

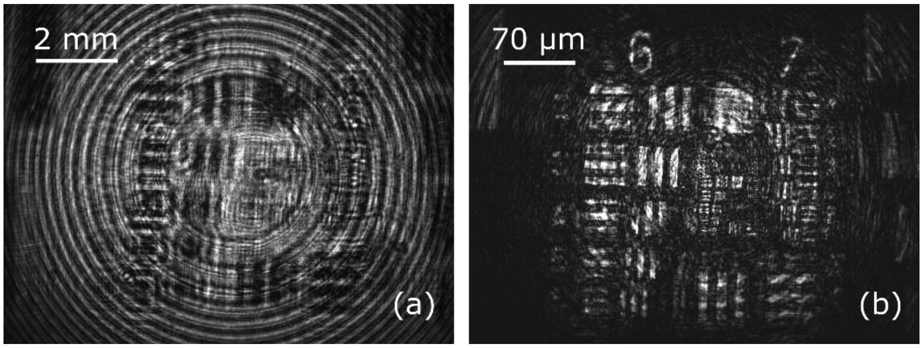

Fig. 1-6. Recorded in-line hologram of an USAF test target using an OPU as the illumination source in panel (a), and the reconstruction of the corresponding contrast hologram in panel (b).

While Fig. 1-7 panel (a) shows the direct reconstruction of the contrast hologram, panels (b), (c), and (d) show the reconstruction by applying standard filtering techniques as the median, NLM, and BM3D, in that order. As seen from the reconstructed images, those conventional techniques do not overcome the influence of the illumination artifacts, and the poor quality is observed in the reconstructed information.

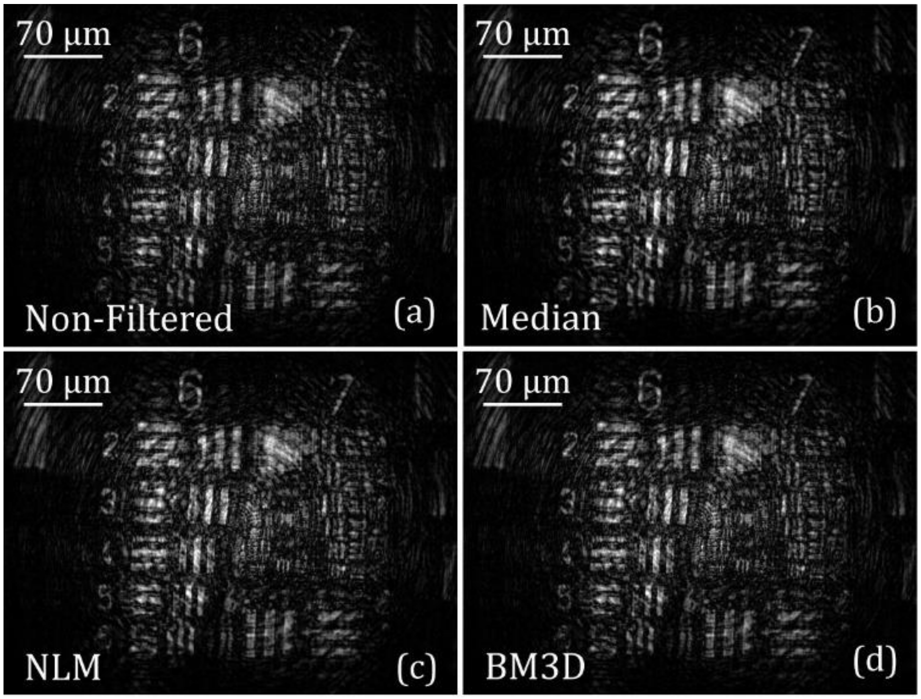

Fig. 1-7. Reconstruction of corrupted DLHM hologram. Direct reconstruction from the contrast hologram in panel (a), after applying median filter (b), NLM filter (c), and BM3D filter (d).

In Fig. 1-8 panel (a), the direct reconstruction of the contrast hologram is compared to Barton’s method and its modification, which are shown in Fig. 1-8 panel (b) and (c), respectively. Although the increased of the contrast of the elements at the outer border of the image, the quality of the visualized USAF test target remains similar to the direct contrast hologram, without improving the effects of the illumination artifacts over the reconstructed image.

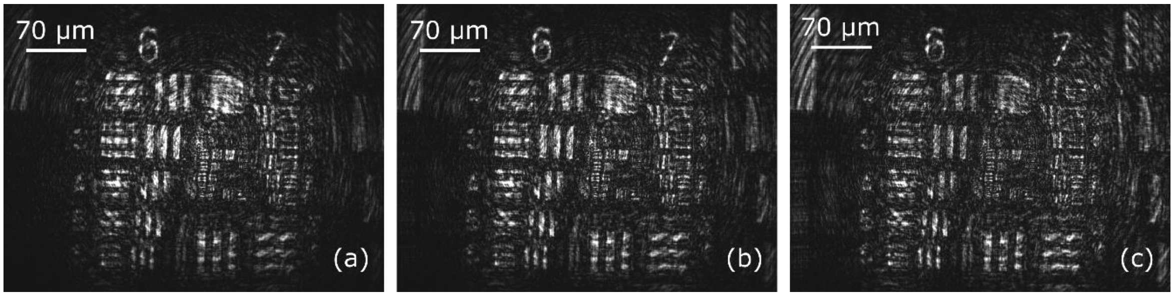

Fig. 1-8. The direct reconstruction from the contrast hologram in panel (a). Panels (b) and (c) show the reconstruction after the application of the Barton's method and its modification respectively.

As it was presented, all the possible point source alternatives bring drawbacks over the recorded in-line hologram mainly due to the presence of artifacts, which constantly affects the final quality of the recovered image in DLHM. The current methods for reducing illumination artifacts in DLHM are not always effective in overcoming all possible artifacts. Therefore, there is a need to develop new methods that can better address this issue.

1.2.3 Occlusions

Sample volume visualization is common for studying micrometer-sized objects, including biological specimens. The observation of swimming specimens in a water volume [14,23,24] and monitoring microplastic contamination [51,52] are tasks that can be named. Instead of regular microscopy imaging techniques that produce in focus plane-by-plane information of the sample volume, DLHM records a digital hologram that carries the scatter information of the whole illuminated volume sample. Moreover, the reconstruction stage offers the possibility of numerical focusing on different planes where various objects may be located. That makes DLHM an attractive technique for sample volume visualization. In DLHM, and as in any regular system for the visualization of volume sample [53,54], it can occur that the information of an illuminated object to be visualized does not reach the recording system, partially or totally, by the interposition of another object in the same line of sight [25]. This phenomenon is known as occlusion. Because DLHM is a holographic technique, the superposition of the diffracted information of both objects can be recorded in the same region of the digital hologram. However, the reconstruction process of DLHM has the capability of numerical refocusing individually the different planes by simply computing eq. (1.3) at different z distances, but the presence of more than one object in the line of sight generates a degradation of the reconstructed image.

Fig. 1-9 (a) shows a recorded hologram of a USAF test target [50] glued to a glass cover slide of epithelial cheek cells. The reconstructions of the said hologram to focus the two different sample planes are shown in Fig. 1-9 (b) and (c).

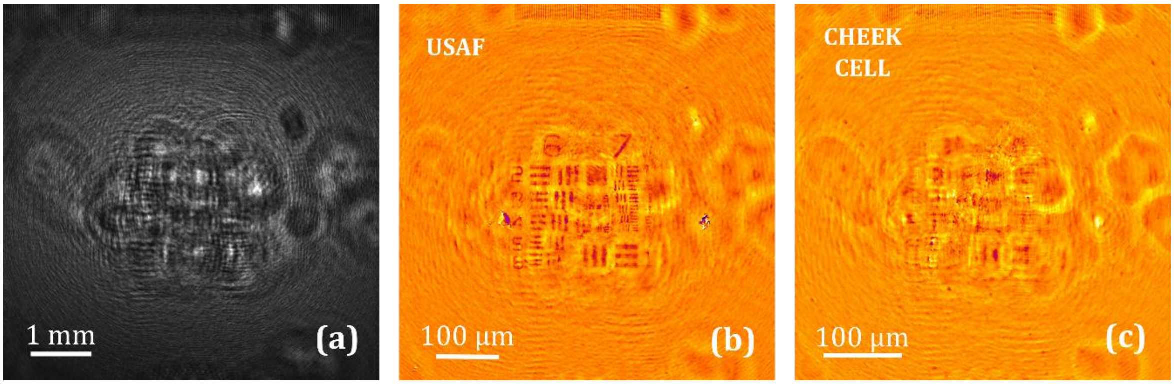

Fig. 1-9. In-line hologram of the occlusion between an USAF test target and epithelial cheek cells in panel (a). Panel (b) and (c) are the reconstructions to get in focus the USAF test target and the epithelial cheek cells, respectively.

As can be seen in Fig. 1-9, the location of different objects in the sample volume renders to partial or total occlusions, compromising the quality of the imaged sample and distorting the sample information with that from the out-of-focus planes. This fact demands for a method to remove the occlusions in DLHM, allowing the visualization of the samples for in-focus different planes without the presence of information of out-of-focus planes.

2. Multiview Correlation Method for DLHM hologram correction

The linearity in amplitude of in-line holograms [55] supports the use of the superposition principle in multiplexing methods, such as the time multiplexing [19] presented in the previous chapter. Inspired by that method, a spatial multiplexing approach to overcome the limitations of DLHM presented in the former chapter is presented.

In this approach, an in-line DLHM hologram $H(x,y)$ can be expressed as a product of different information $I_1(x,y)$ and $I_2(x,y)$,

$$H(x,y) = I_1(x,y)I_2(x,y)\,, \tag{2.1}$$

where $I_1(x,y)$ is the information of the scattered light from a static specimen placed at z distance from the point source and $I_2(x,y)$ is deeply dependent of the application of this method and will be explored in the following chapters; it could be an illumination inhomogeneity, the occluding information of an object, among others. For this method to work, a set of in-line DLHM holograms is recorded while the static specimen is located at different positions across its plane as

$$H_i(x,y) = I_1\big(x-\Delta x_{i,1}, y-\Delta y_{i,1}\big)I_2\big(x-\Delta x_{i,2}, y-\Delta y_{i,2}\big). \tag{2.2}$$

$\Delta x_{i,1}$and $\Delta y_{i,1}$ are the displacements in the *x*-axis and *y*-axis of the specimen over the sensor plane in $I_1(x,y)$ for each i^{th} recorded in-line DLHM hologram; and $\Delta x_{i,2}$and $\Delta y_{i,2}$ are the same for $I_2(x,y)$. The recording of multiple in-line DLHM holograms of the same specimen allows for obtaining, in overall, a set of holograms with the same information under different conditions [56]. This method aims to separate $I_1(x,y)$ and $I_2(x,y)$ to overcome the identified limitations of DLHM.

A new composite hologram is produced by the coordinated addition of the set of in-line DLHM holograms. To achieve this, the normalized cross-correlation (NCC) is evaluated to determine the relative displacement between the set of recorded holograms [57]. A hologram of the set, it is chosen as fixed recording for the calculation of all NCC with respect to it. A region of interest of this hologram, with its origin of coordinates in $(x_{T_{Fix}}, y_{T_{Fix}})$ and size $\left(\nabla x_{T_{Fix}}, \nabla y_{T_{Fix}}\right)$, is selected as the template $T(x', y')$ for the computation of the NCC. The search for the template $T(x', y')$ on each of the recordings of the set of in-line DLHM holograms $H_i(x, y)$ constitutes the computation of the NCC matrix, following the expression [57]:

$$NCC(x, y) = \frac{\sum_{x',y'} T(x', y') \cdot H_i(x, y)}{\sqrt{\sum_{x',y'} T(x', y')^2 \cdot \sum_{x',y'} H_i(x, y)^2}}. \tag{2.3}$$

From the NCC matrix, the coordinates of the correlation maximum $(x_{NCC_{Max}}, y_{NCC_{Max}})$ mark the position where the template has the largest similitude with the corresponding displaced hologram. These coordinates account for the relative shift between the displaced hologram and the template. Therefore, the relative displacement between the fixed and each of the holograms of the set is computed as

$$(\Delta x_S, \Delta y_S) = \left(x_{T_{Fix}} - x_{NCC_{Max}}, y_{T_{Fix}} - y_{NCC_{Max}}\right). \tag{2.4}$$

The composite hologram $H_{Comp}(x, y)$, is produced by the coordinated addition of the in-line DLHM holograms $H_i(x, y)$ considering their relative displacement previously calculated:

$$H_{Comp}(x, y) = \sum_{i=1}^{N} H_i(x + \Delta x_{i,1}, y + \Delta y_{i,1}). \tag{2.5}$$

If equation (2.2) is replaced in equation (2.5), the relative displacements of $I_1(x, y)$ are removed, and it can be separated from the sum, allowing the conservation of this information as:

$$H_{Comp}(x, y) = I_1(x, y) \sum_{i=1}^{N} I_2\left(x - \Delta x_{i,2} + \Delta x_{i,1}, y - \Delta y_{i,2} + \Delta y_{i,1}\right). \tag{2.6}$$

As $I_2\left(x - \Delta x_{i,2} + \Delta x_{i,1}, y - \Delta y_{i,2} + \Delta y_{i,1}\right)$ has a different relative displacement for all the holograms of the set. In following chapters this equation will be known as the composition equation.

For a given number of N added holograms the term inside the summation becomes a homogeneous quantity, resulting in a corrected hologram that contains, in overall, only the information of $I_1(x,y)$:

$$H_{Comp}(x,y) \approx I_1(x,y)\,. \tag{2.7}$$

The same addition can be performed to a set of reference holograms, generating a composite $R_{Comp}(x,y)$.

A normalization is computed for both $H_{Comp}(x,y)$ and $R_{Comp}(x,y)$ by dividing each resulting pixel by the number of added in-line holograms/references utilized for its composition. Both images are pixel-wise subtracted to produce the composite contrast hologram [58].

$$\tilde{I}_{Comp}(x,y) = I_{Comp}(x,y) - R_{Comp}(x,y). \tag{2.8}$$

Finally, $\tilde{I}_{Comp}(x,y)$ is reconstructed by the numerical implementation of equation (1.3) as was presented in the former chapter.

The logo of the Opto-Digital Processing Research Group (ODP) and a dragonfly silhouette are used for applying the Multiview Correlation Method to illustrate its performance in correcting holograms. Both objects are displaced over a gray background simulating the recording of the set in-line holograms. The displacements for the objects are different as a requirement for the application of the proposed method. In a fixed image of the set, a region of the ODP logo is selected as the template, as is shown in Fig. 2-1 (a). The NCC between the set of displaced images and the template is computed to determine the position of this template in each of the images of the set in Fig. 2-1 (b).

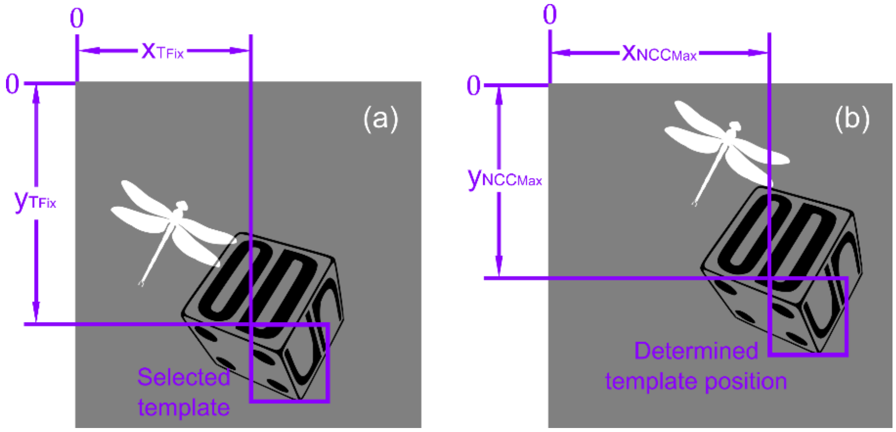

Fig. 2-1. Selected template coordinates for a fixed displaced image, in panel (a) and one displaced image of the set, in panel (b).

As the coordinates of the template in the fixed image $(x_{T_{Fix}}, y_{T_{Fix}})$ are known, the coordinates of the template in the set of images are subtracted to determine the relative displacement $(\Delta x_s, \Delta y_s)$ for all the images of the set. Then the coordinated addition considering the relative displacements is computed. Fig. 2-2 shows this addition of two images; the information about the ODP logo is located and added in its position, given the determination of the template coordinates. Conversely, as the relative displacements of both objects are different, the information about the dragonfly does not coincide, generating a fuzzy addition of this object information. Additionally, a larger image size is observed produced by the displacement of the images.

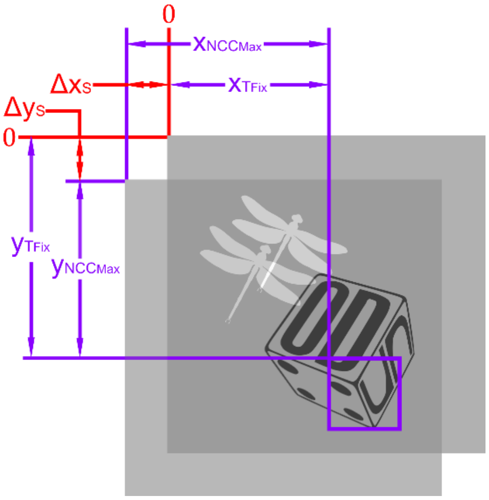

Fig. 2-2. Relative displacements between an image of the set and the one fixed.

When more displaced images are added, the undesired information, the dragonfly information in this case, becomes fuzzier, while the desired information is preserved. This can be seen in Fig. 2-3 (a) where 25 images are added to compose the image. Finally, to eliminate the presence of the edges of the composite image, each resulting pixel is divided by the number of added images utilized for its composition, resulting in the corrected image showed Fig. 2-3 (b) with a larger size than that of the original image.

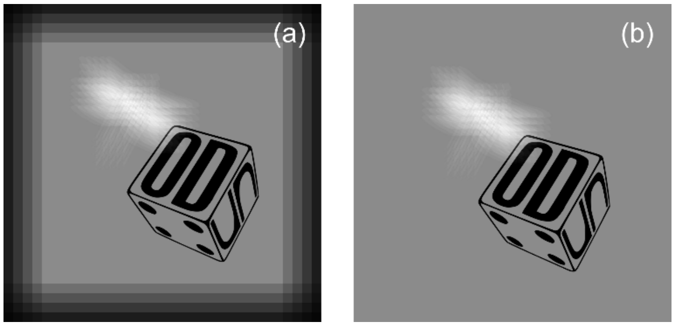

Fig. 2-3. Composite image in panel (a) and its normalization in panel (b).

The application and effectiveness of the Multiview Correlation Method to eliminate undesired information while the desired one is conserved is presented. In following chapters, this method will be applied over recorded in-line holograms to overcome identified limitations in DLHM

3. Improvements in the Numerical Aperture and FOV of DLHM

The illumination NA was identified in Section 1.2.1 as the parameter inherited from the hardware that limits the performance for the visualization of samples in DLHM. It depends on the source of spherical wavefront illumination and is essential for determining the performance and arrangement of the DLHM setup. Furthermore, the NA and the source-to-sample distance limit the FOV for visualizing samples in DLHM. This chapter presents a characterization method for the reliable measurement of the NA and a method for the extension of the FOV for DLHM. Ultimately, the integration of both developments leads to a cost-effective microscope with improved capabilities and without increased cost.

3.1 Numerical Aperture measurement

The search for alternatives to pinhole-based illumination has led to the fabrication of point sources, such as optical fiber cone tips or holographic point sources, requiring the grading of their NA value. This search has also resulted in the use of low-cost elements, such as aspheric or diffractive-refractive lenses, with low-reliable graded values of NA. Because the performance of DLHM is strongly supported in the *NA* of the illuminating light source, a reliable characterization of the NA of their produced propagating light beams is needed.

The closest theoretical model for the experimental illumination sources is the Gaussian beam approach [15]. As the intensity distribution $I(x,y,z)$ is centered at (x_0,y_0) coordinates a Gaussian beam profile is expressed as:

$$I(x,y,z) = A_0 \exp\left[-\frac{(x-x_0)^2+(y-y_0)^2}{\omega^2(z)}\right], \qquad (3.1)$$

where A_0 is the amplitude of the intensity distribution in the position (x_0,y_0), and ω is the beam width at z distance from the beam waist [59].

In the presented method, the intensity distribution of the illumination source is recorded over two positions separated a distance Δz across the optical axis as is shown in Fig. 3-1. Using this figure, a geometrical analysis leads to an expression for the divergence angle θ as:

$$\theta = \arctan\left(\frac{\Delta\omega}{\Delta z}\right). \tag{3.2}$$

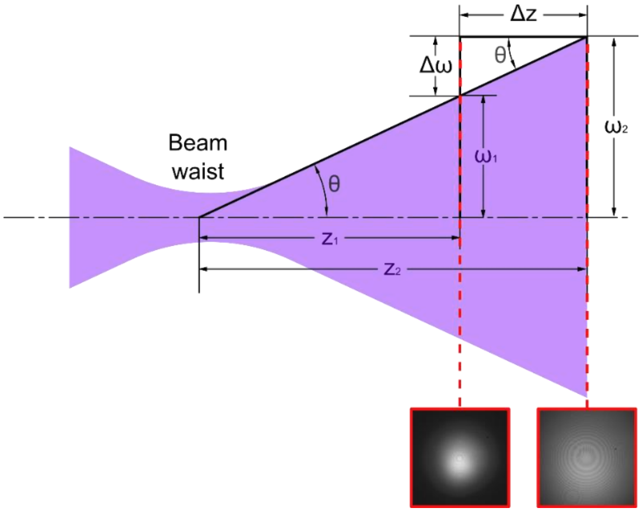

Fig. 3-1. Divergence of a Gaussian beam.

Both recorded intensity distributions, such as the one shown in Fig. 3-2 panel (a) for the illumination produced by a SM600 optical fiber, are fitted to a bidimensional Gaussian distribution by the Levenberg-Marquardt non-linear algorithm [60], such as the one shown in Fig. 3-2 panel (b). In panels (c) and (d), the intensity profiles along the x_0 and y_0 axis are presented to illustrate the comparison between the recorded and fitted distributions. From these fitted Gaussian distributions for both recordings, the standard deviations σ_1 and σ_2 are determined.

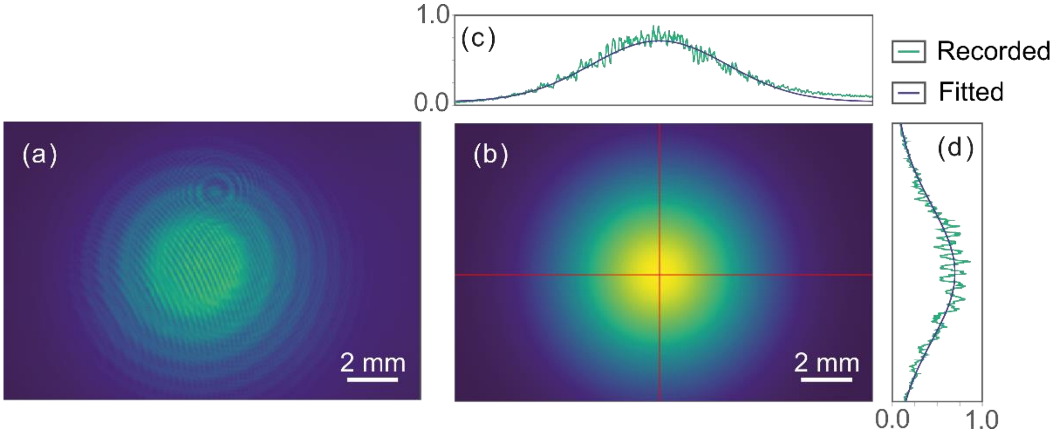

Fig. 3-2. Intensity distribution for a propagating Gaussian light beam produced by a SM600 optical fiber. (a) Normalized recorded intensity. (b) Numerical estimation of the Gaussian beam distribution of panel (a). Panels (c) and (d) are the intensity profiles for the recorded and fitted distributions along x_0 and y_0, respectively.

As the beam width can be expressed as $\omega(z) = 2\sigma(z)$ [26], equations (1.7) and (3.2) can be used to rewrite an expression for the NA of a Gaussian intensity distribution as it is propagated over a distance Δz as:

$$NA = n \sin\left[\arctan\left(\frac{2\Delta\sigma}{\Delta z}\right)\right] \tag{3.3}$$

To summarize, the direct illumination of a digital camera is recorded for two positions displaced a distance Δz. The minimization by the Levenberg-Marquardt non-linear algorithm is performed over the recorded illumination distributions by fitting them to a Gaussian profile distribution. From the Gaussian distributions, the standard deviations $\sigma_1$and σ_2 are determined and subtracted to find $\Delta\sigma$. Finally, using the values of Δz and $\Delta\sigma$, and the refractive index of the medium where the beam is propagated, are used to determine the NA of the illumination source utilizing equation (3.3).

The performance of the proposed method was tested on numerically modeled light beams, which yielded a R-square factor of 0.99. And also was validated by experimentally characterizing graded illumination sources. Using the method, the illumination of a calibrated aspherical lens C105TMD-A with a graded NA of 0.6 was characterized, resulting in a NA of 0.587±0.044 was the reported value, indicating a 2.16% error percentage compared with the reported value by the manufacturer. And also, the output illumination cone for two optical fibers were characterized. For a SM600 optical fiber with a reported range of NA between 0.07 and 0.11, the characterized NA was 0.082±0.011; and for a SM450 with a reported range of NA between 0.08 and 0.12, the characterized NA value using the method was 0.083±0.011. Both illumination cones of the optical fibers were in the graded ranges indicated by the manufacturer. These results demonstrate the effectiveness of this method in accurately measuring the NA of propagating Gaussian light beams, supporting its application in the characterization of illumination light sources in DLHM.

The theoretical analysis, implementation, and testing of this method was reported in the following manuscript, attached at the end of this text:

"*Automatic method to measure the numerical aperture of a propagating Gaussian light beam*", Óptica Pura y Aplicada **55**, 1-8 (2022) [26].

Additionally, this work was presented in the following conference:

"Método automático para la medición de la apertura numérica de haces de luz Gaussianos", XVII Encuentro nacional de Óptica y XIII Conferencia Andina y del Caribe en Óptica y sus aplicaciones, Medellín Colombia, 2021 [28]

3.2 Expanding of the field of view for DLHM

The FOV is a fundamental parameter in visualizing both biological and non-biological specimens for DLHM, indicating the maxima imaging covered area. Fig. 3-3 shows the variation of the FOV depending on the source-to-sample distance z for different values of NA according to equation (1.11). It is clear from this plot that the closer the sample is to the point source, the smaller the FOV of the visualized sample. This leads to a greater magnification of the diffraction pattern, ensuring correct sampling on the digital sensor.

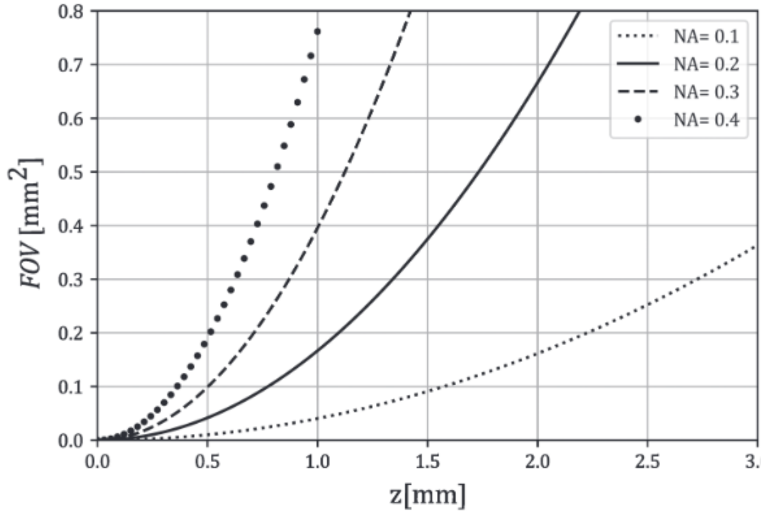

Fig. 3-3. Behavior of the FOV as the source-to-sample distance z is varied for different NA values.

Visualizing biosamples, such as red blood or epithelial cells, requires a smear preparation [9]. For those specimens, a larger FOV is preferred, given that the larger the FOV, the more cells of the smear can be visualized. The increase of the FOV implies an increase in the source-to-sample distance, jeopardizing the correct sampling of the higher frequencies of the diffracted pattern; this condition demands the search for a method to enlarge the FOV with no decrease of the sampling capabilities of the recording system.

In the literature, there is a method to expand the FOV in DLHM, that by means of a digital micromirror device (DMD), displaces the point source over its plane to illuminate the sample from different directions [17]. One way to simplify this method is to use x-y micrometer screws instead of the DMD to displace the point source over its plane; in all cases, these approaches require additional elements in the point source setup, resulting in a more complex and bulkier optical setup.

A simpler approach that no requires additional components can be made by displacing the sample over its plane a distance of d_x using a conventional microscope stage, as illustrated in Fig. 3-4 (a). This movement generates a displaced projection of the diffraction pattern over the recording plane according to the magnification relation $D_x = \frac{d_x z}{L}$, as shown in the recorded holograms in Fig. 3-4 (b). As explained in the previous chapter, a digital computation of the NCC is used to determine the displacement D_x. In order to apply the NCC, an overlap region S_d is needed between the recordings, where a template can be defined as is shown in Fig. 3-4 (c).

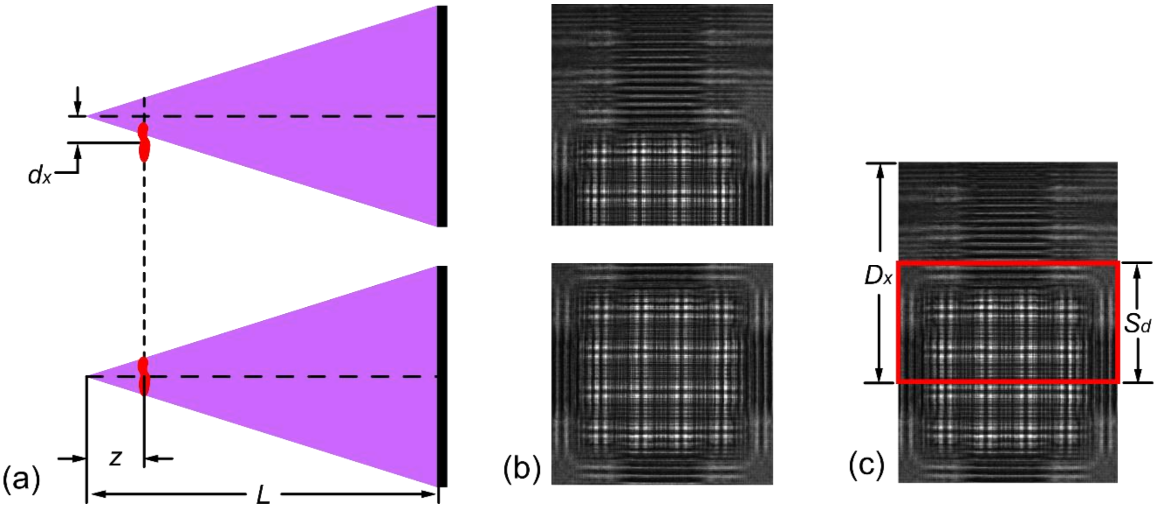

Fig. 3-4. Displacement of the sample in panel (a). Comparison between the recorded holograms in panel (b), and their overlapping region in panel (c).

A set of in-line holograms is recorded while the sample is displaced over its plane, as was previously presented. A new composite hologram with an extended field of view is produced by coordinately superimposing the recorded in-line holograms by accounting the estimated displacements. The same process is repeated for the reference to generate a composite reference. However, due to the non-uniformed background in the composition, a contrast hologram is generated to eliminate undesired edges in the composite hologram. Barton's method [22] and its modification [18] also overcome the lack of homogeneity of the background and can be performed.

The illustration of the proposed method for expanding the FOV was tested with holograms recorded in a DLHM microscope built with an aspherical lens of $NA = 0.6$ illuminated with a 405 nm plane wave. The resulting point source at its focal point illuminates a reticle calibration test placed at 0.69 mm from the point source. A digital camera with 2048x2048 square pixels of 3.8 μm in side length records the in-line holograms; the center of the camera is 18.96 mm away from the said source. In the reconstruction stage, the modified Barton method [18] was applied over the respective holograms to avoid inhomogeneities illumination wavefront. Fig. 3-5 (a) shows the reconstruction of a single hologram recorded with the built microscope achieving a FOV of 0.08 mm^2. Fig. 3-5 (b) shows the reconstruction of the hologram composed by 9 single holograms with an overlap of $S_d \approx 1100$ pixels of length measured in the recording plane and achieving a FOV of 0.287 mm^2. After applying the proposed method, the FOV enlargement is 258%; see the outer area beyond the dashed-red square in Fig. 3-5 (b).

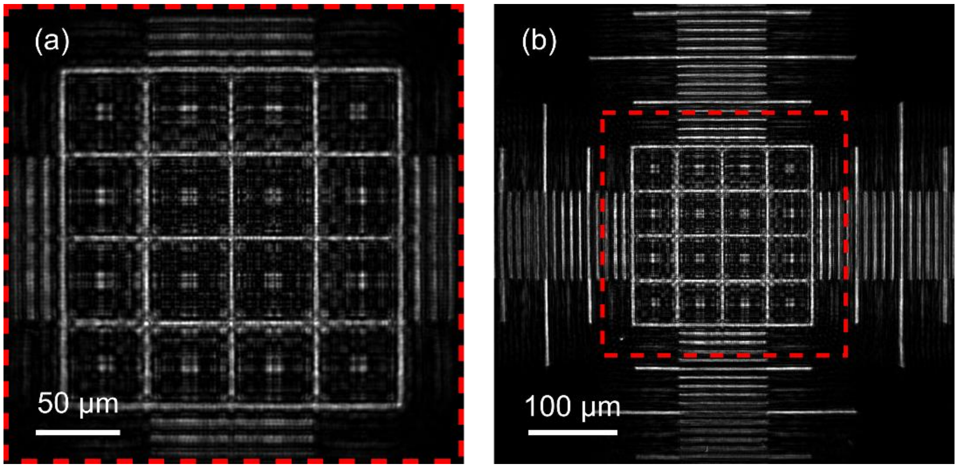

Fig. 3-5. Visualization of a calibration test target. Panel (a) is the reconstruction of the central recorded in-line hologram and panel (b) is the reconstruction of the composite hologram generated with the proposed method for expanding the FOV.

3.3 The most cost-effective DLHM

Microscopy visualization of samples is commonly related with biological applications. Studies of micrometer-sized biosamples are presented at all educational and professional levels. Since the first approach of the cell structure in basic education, through the detection of diseases, and finishing in research application, for all those possible applications, microscopes are a fundamental tool. However, for all those levels, the access to microscopic technologies is limited to the well-funded laboratories, universities and schools given the expensive cost of optical elements and labels. Nevertheless, access to microscopy technologies is restricted to well-funded laboratories, universities, and schools due to the expensive cost of optical elements and labels. Consequently, it is imperative to explore the possibility of acquiring cost-effective microscopes that offer high performance for visualizing micrometer-sized biosamples. Increasing access to microscopy equipment can facilitate the development of new hands-on approaches for educational purposes, enhance disease detection and diagnostics for medical centers with limited funding, among other benefits.

As presented before, DLHM is a simple holographic technique that only requires a point source of spherical waves and a digital camera to work. This simplicity in the hardware has allowed for the development of cost-effective microscopes that use DLHM technology. The Optics and Opto-Digital Processing Research Group (ODP) recently developed the most cost-effective holographic microscope to date in 2021, costing approximately US$53 [2]. The hardware consists of a plug-and-play aspheric lens with a graded NA of 0.6 (US$4.70), integrated with a 650 nm laser diode of 5mW (US$1.33) to generate the spherical wavefront illumination, and for the recording of holograms, a surveillance camera with 2592x1944 square pixels of 2.2 μm in size (US$43.40). The microscope is supported on a 3D-printed body and commercial screws and nuts, including the displacer for the system alignment and the sample stage (US$2.6).

When a microscope is designed, it is crucial to accurately characterize the optical elements used in the setup. The two main parameters that determine the microscope setup are the size of the digital sensor and the NA of the illumination. The digital sensor size is determined by the commercial sensor, which in this case is (5.7 x 4.2) mm. And the NA of the illumination of the low-cost aspheric lens was validated by the proposed method to measure the NA with a value of 0.578.

This microscope was presented in the following conference and its proceeding is attached at the end of this text:

“Cost-effective digital lensless holographic microscope," in OSA Imaging and Applied Optics Congress (Online), Washington DC United States, 2021 [29].

As can be identified, the most expensive cost for building this microscope is the digital camera. The market offers commercial sensors with a lower cost, such as the Raspberry Pi Camera V1 (RaspiCam) for an amount of $US2.83 with the same format of (2592 x 1944) square pixels but a reduced sensor size of (3.62 x 2.72) mm. As it was presented in the former subsection, a reduction in the sensor size leads to a reduction in the performance of the system for visualized microscopic samples. In that regard, the proposed method for expanding the FOV in DLHM was used to test the feasibility of replacing bigger digital sensors with a sensor with smaller sizes without implying a reduction in the optical performance of the DLHM microscope.

The proof of concept was validated by the imaging of a phase USAF test target [50] utilizing a research camera DMM 37UX250-ML (TISCam) with a sensor size of (8.44 x 7.06) mm with a format of (2448 x 2048) square pixels. The setup where the expanding method was presented in section 3.2 was utilized for this validation. In Fig. 3-6, the numerically reconstructed images of the USAF test target are shown. Panel (a) shows the direct reconstruction of the recorded hologram using TISCam with a FOV of 0.286 mm^2. Panel (b) shows the reconstruction of the central single hologram with a FOV of 0.051mm^2. And panel (c) shows the reconstruction of the composite hologram, with the same FOV of panel (a), resulting from applying the method for extending the FOV with 9 holograms for the composition. Those latter reconstructions were recorded using RaspiCam. After applying the proposed method, the FOV enlargement is 460%; see the outer area beyond the dashed-blue square in Fig. 3-6 (c). For TISCam, element 3 of group 8 is visualized, implying an achieved resolution of 1.55 µm, while element 1 of group 8 is visualized for RaspiCam achieving a resolution of 1.95 µm.

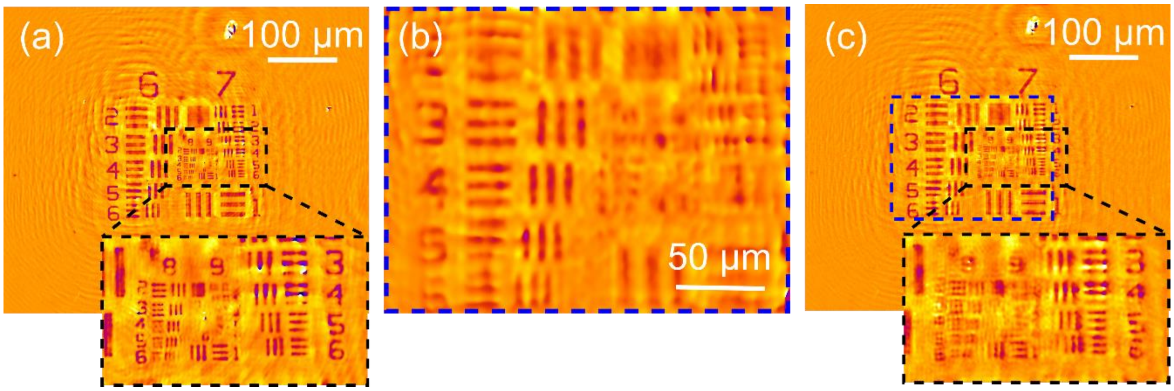

Fig. 3-6. Comparison between the phase reconstruction of an USAF test target. Panel (a) shows the reconstruction of an in-line hologram that was recorded using TISCam. Panel (b) shows the reconstruction of an in-line hologram recorded using RaspiCam. Panel (c) shows the reconstruction of a composite hologram that was recorded using RaspiCam and was composed by the proposed method.

The difference between the achieved resolution for the reconstruction of the TISCam hologram and the reconstruction of the composite hologram was 0.5µm. The proposed method for expanding the FOV using holograms recorded with the RaspiCam yields comparable results to those achieved by recording the information using the TISCam. The decrease in the cost of the digital camera, in conjunction with the application of the expansion of the FOV method, will take further the development of super low-cost microscopes without sacrificing the performance of the reported microscopy systems.

4. Overcoming the presence of illumination artifacts

As was presented in section 1.2.2, the presence of artifacts inhered from the illumination source reduces the quality of the visualized microscopic images. The reported methods to overcome inhomogeneities in the illumination for DLHM only work for some of the illumination or reflective artifacts presented in the hologram recording stage of DLHM. In this chapter, the Multiview Correlation Method introduced in Chapter 2 is utilized to overcome the presence of any artifact inherent to the illumination source, including the reflective artifacts just said.

In the correction of the illumination artifacts approach, the set of recorded in-line DLHM holograms, needed for the application of the Multiview Correlation Method, contains two information, the sample information $I_S(x,y)$ displaced over the FOV and the static illumination artifacts $A(x,y)$. Knowing that, equation (2.2) can be rewritten as:

$$H_i(x,y) = I_S(x-\Delta x_i, y-\Delta y_i)A(x,y). \tag{4.1}$$

The chosen template for applying the Multiview Correlation Method must include the information of the sample and appears in all the in-line holograms of the set. In the application of the proposed method, the sample information is conserved while the artifacts information is displaced as it is indicated in the composition equation:

$$H_{Comp}(x,y) = I_S(x,y)\sum_{i=1}^{N} A(x+\Delta x_i, y+\Delta y_i). \tag{4.2}$$

Finally, the coordinated addition of in-line DLHM holograms presented in the above summation, turns the information about the artifacts into a homogeneous distribution preserving only the sample information:

$$H_{Comp}(x,y) \approx I_S(x,y). \tag{4.3}$$

The effectiveness of this method for correcting the artifacts inherited from the illumination has been illustrated utilizing one of the seminal Gabor's holograms [61]. A strong artifact in the illumination source has been simulated by intentionally adding a black spot to the in-line hologram, as illustrated in Fig. 4-1 (a) and (b). The ruining effect of the illumination artifact moves around the recorded intensity simulating the sample displacement, given that the relative displacements can be associated with the information of the sample or the illumination, as can be seen in equations (4.1) and (4.2). This strong artifact removes valuable information from the in-line hologram that must be somehow recovered. The reconstruction of the in-line hologram in panel (b), shown in panel (c), presents a loss in the quality of the recovered information produced by the simulated perturbation in the illumination.

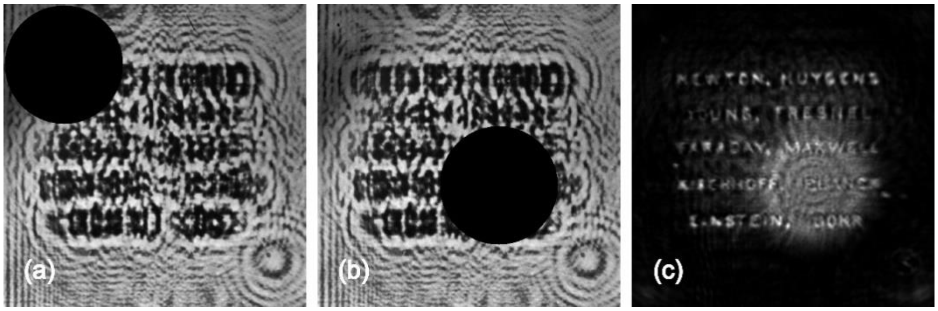

Fig. 4-1. Two simulated corrupted Gabor's in-line holograms in panels (a) and (b). The reconstruction of panel (b) is shown in panel (c).

The composition was performed using the 16 disturbed holograms showed in Fig. 4-2 panel (a). In the composition, the information about the perturbation is added with different relative displacements, and progressively its summations tend to a constant value representing a homogeneous background in the corrected in-line hologram. In Fig. 4-2 panels (b) and (c), the corrected in-line hologram $H_{Comp}(x, y)$ and its corresponding numerical reconstruction are shown, respectively. In the case of this simulation, the application of the proposed method produces a corrected hologram that tends to the original seminal Gabor's hologram.

Fig. 4-2. The set of simulated perturbed holograms is shown in panel (a). The corrected Gabor's in-line hologram and its corresponding reconstruction are shown in panels (b) and (c), respectively.

As was presented in section 1.2.2, the diffractive-refractive lenses create a highly contrasted ring-like structure over the illumination wavefront, causing a strong inhomogeneity in the illumination. Up to the best knowledge of the author, these ring-like structures are the most challenging illumination artifacts in DLHM, making it a suitable test for evaluating the effectiveness of the correction method. To test the proposed method, a Blue-ray optical pick-up unit (OPU), with its integrated diffractive-refractive lens with 0.85 of NA, was utilized to generate a point source with the mentioned strong illumination artifacts. The 405 nm laser of the OPU was used to illuminate a digital camera with (4640 x 3506) square pixels of 3.8 µm in side, which was located at 22.40 mm away from the said source. The RMS contrast

$$C_{rms} = \sqrt{\frac{1}{\sum_{i=1}^{N} w_i} \sum_{i=1}^{P} w_i \frac{(l_i - Lu)^2}{Lu^2}}, \tag{4.4}$$

was evaluated to determine the number N of needed in-line DLHM holograms to compose and the displacements between them to recover the ruined information due to the ring-like structure. The RMS contrast was measured over the circular region of interest (ROI) of radius $\rho = 500$ pixels, and center (x_c, y_c) of the reference recorded showed in Fig. 4-3 panel (a). In equation (4.4), $w_i = 0.5\left\{cos\left[\frac{\pi}{\rho}\sqrt{(x_i - x_c)^2 + (y_i - y_c)^2}\right] + 1\right\}$ is the weight of a raised cosine windowing function, l_i is the luminance at the pixel (x_i, y_i), $Lu = \frac{1}{\sum_{i=1}^{P} w_i} \sum_{i=1}^{P} w_i l_i$ is the local weighted luminance at the circular ROI, and P is the number of pixels within it; further information about this RMS contrast measurement can be found in reference [62]. The reduction in the RMS contrast was evaluated as the number of recorded holograms and the distance between them varied. Six neighborhood layouts were evaluated to choose the suitable layout and the displacement value d between the holograms in the recording plane, as shown in panel (b) of Fig. 4-3. The selected neighborhood layout determines the N scanned images; $N = 9$ for first neighbors (NBHD 1), $N = 25$ for second neighbors (NBHD 2), $N = 49$ for third neighbors (NBHD 3), $N = 17$ for A neighbors (NBHD A), $N = 17$ for B neighbors (NBHD B), and $N = 15$ for C neighbors (NBHD C).

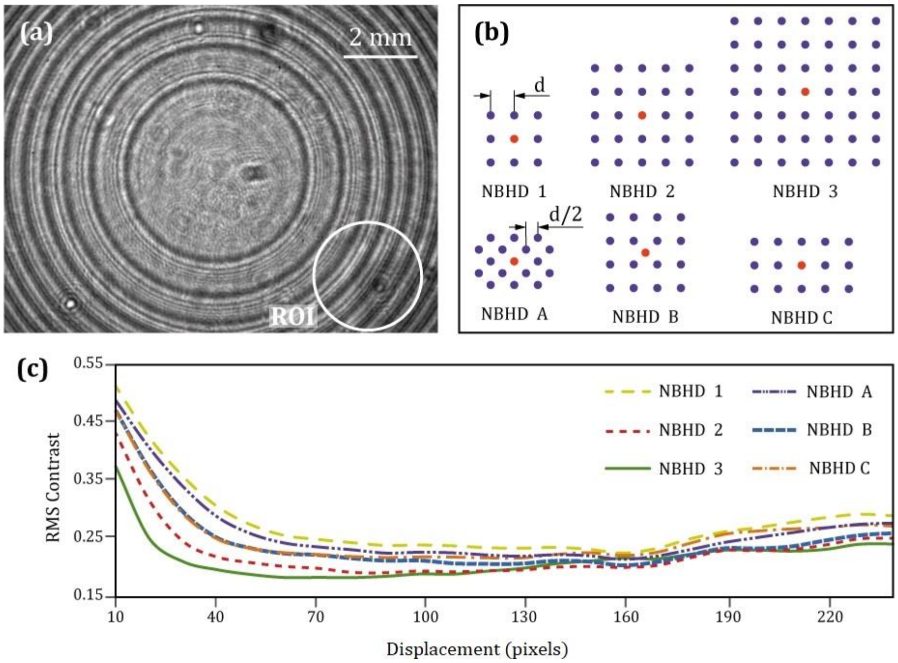

Fig. 4-3. Panel (a) shows the region of interest where the contrast is measured. Panel (b) is an illustration of the six neighborhood layouts evaluated. The evolution of the RMS contrast as the distance between the recorded holograms is varied, for each neighborhood layout, is shown in panel (c).

The behavior of the RMS contrast in the selected ROI is shown in panel (c) of Fig. 4-3. This figure shows the decay in contrast for various neighborhood layouts and the distance between the recorded holograms. NBHD 3 shows the most significant RMS contrast decay, using 49 recorded holograms for the composition. As the difference of the contrast decay between NBHD 2 and 3 is not very relevant, can be chosen NBHD 2 because in this way the number of needed images is reduced to 25. Over the plot for the NBHD 2, dashed-red line in panel (c) Fig. 4-3, can be read that a distance around 80 pixels between the holograms in the recording plane, leads to the best reduction of the contrast of the ring-like structed that ruins the reconstructed images.

The USAF test target [50] presented in Section 1.2.2 to illustrate the artifacts limitations in DLHM, was located at 0.25 mm from the source of the built microscope. A x-y translation stage with standard micrometer screws was used to record the 25 holograms with displacements of 80 pixels measured in the digital camera plane, as was determined by the previous RMS contrast evaluation. The reconstruction of the contrast hologram is shown in Fig. 4-4 (a); the ring-like structures ruin the reconstructed image, hiding important details of the imaged sample, as was previously presented in Section 1.2.2. Panel (b) shows the direct reconstruction of the composite hologram resulting from the composition of 25 holograms 80 pixels apart. The improvement of the reconstructed image is observed, as group 7 is fully visible, and group 8 is also partially observable. Further improvement can be reached as the modified Barton's method [18] is applied to the composed hologram. The outermost details of the target become visible, and an improvement of the contrast is reached, as is seen in panel (c). A zoom-in of the area inside of the red dashed-line square in panel (c) is presented in panel (d), where group 8 becomes visible, indicating the effectiveness of the proposed method.

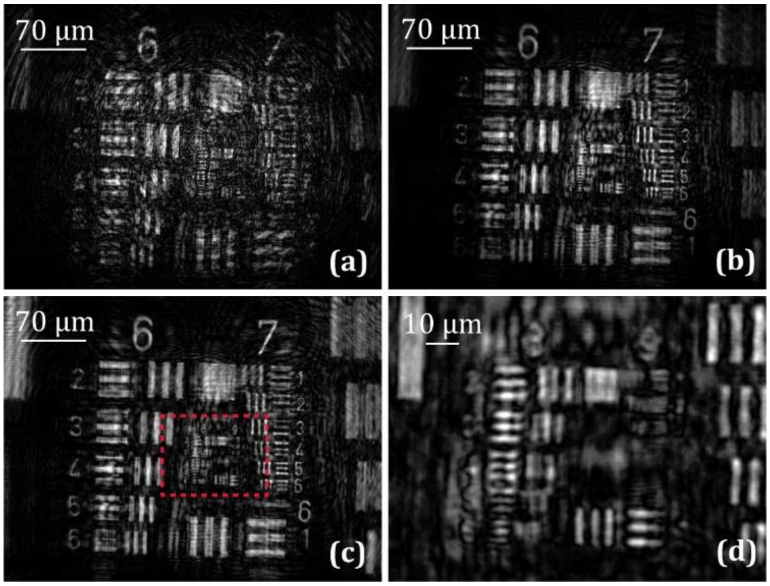

Fig. 4-4. Comparison of the direct reconstruction from the contrast hologram in panel (a), the proposed method in panel (b), and the proposed method in conjunction with the modified Barton's method in panel (c). Panel (d) shows a zoom-in of the area inside of the red dashed-line square, highlighting groups 8 and 9.

In the same microscope, a section of the head of a drosophila melanogaster fly, with internal complex structure, was utilized as sample. The recorded in-line hologram is shown in panel

(a) of Fig. 4-5. The presence of the strong ring-like structure of the illuminating wavefront is clearly visible in the in-line hologram. The net effect of this perturbation is also evident in the reconstructed image in panel (c) and the corresponding zoomed-in area in panel (e). The application of the proposed method leads to the composite hologram shown in panel (b). The effectiveness of the composition is apparent in the erasing of the strong ring-like structure; the composite hologram presents a remaining ripple structure that does not perturb the area that contains the information of the sample. These facts become visible in the reconstructed image shown in panel (d). The ring-like structure that can be observed in panel (c) is no longer present in the reconstruction of the composite hologram, as it is highlighted in the zoomed-in area presented in panel (f). In contrasting panels (e) and (f), the effectiveness of the proposed method is even more notorious for eliminating the illumination artifacts in the holograms and, therefore, in the corresponding reconstructions.

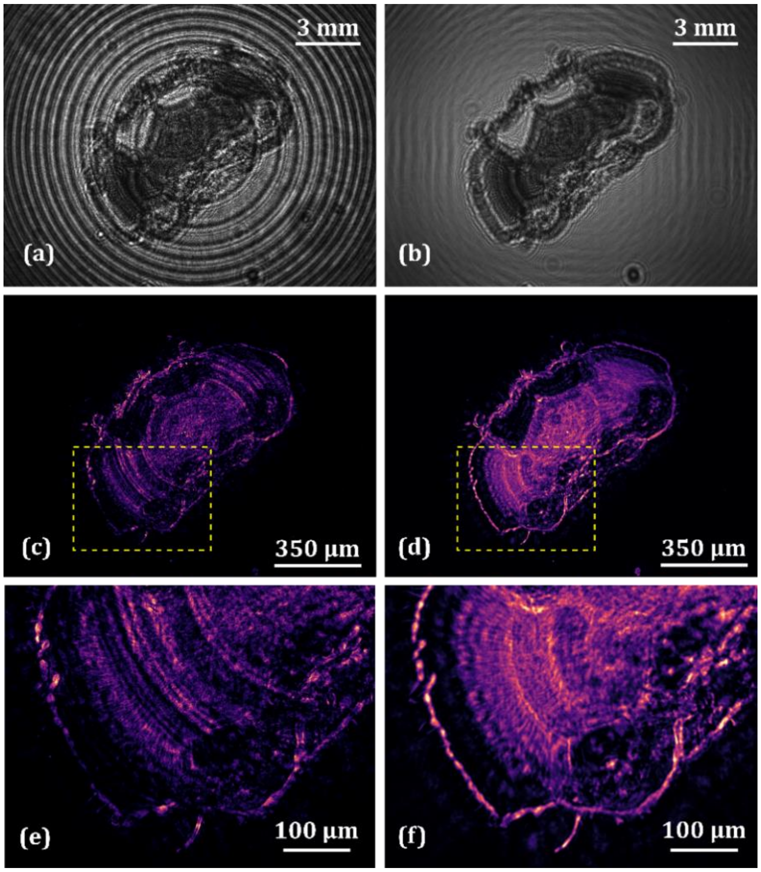

Fig. 4-5. Section of the head of a drosophila melanogaster fly imaged in DLHM. Panel (a) is the recorded in-line hologram and panel (b) the hologram generated with the proposed method. Panel (c)/(d) shows the reconstruction of the hologram in panel (a)/(b). Panel (e)/(f) shows the zoomed-in image of the yellow-dashed rectangle area in panel (c)/(d).

Finally, to overcome the artifacts produced by reflections of the illumination presented in Section 1.2.2, a regular pinhole-based illumination DLHM was built. The illuminating point source was made with a collimated laser with a wavelength of 532 nm focused on an 8 µm diameter pinhole. Panel (a) of Fig. 4-6 shows the reconstruction of the tip of an imaged acupuncture needle, where the ring-like structure is evident all over the surface of the reconstructed object. The application of the method presented in this section is shown in panel (b), where the ring-like structure is eliminated from the sample surface. And finally, a 100 µm circle from a calibration microscopy slide was imaged to show the effectiveness of this method for eliminating reflective artifacts. As was presented before in Section 1.2.2, a close distance between the pinhole and the sample slide produces reflective artifacts that affect the quality of the reconstructed image of the sample. Panel (c) of Fig. 4-6 shows the direct contrast hologram reconstruction of the microscopy calibration circle where the undesired reflective artifact can be seen. In contrast, panel (d) of the same figure presents the reconstruction after applying the proposed method, where it can be observed that the reflective artifact is eliminated. Clearly, the proposed method effectively reduces illumination and reflective artifacts, leading to an improved reconstruction with no effects of the artifacts over the visualized images.

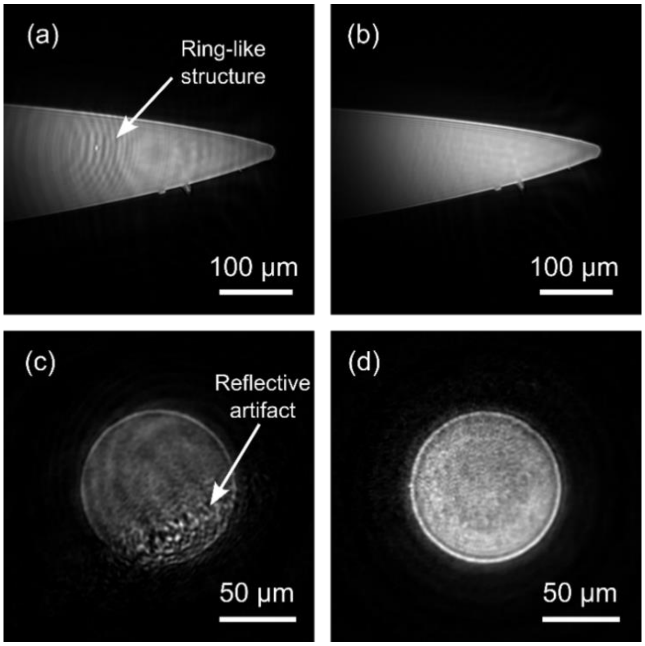

Fig. 4-6. Panel (a)/(b) is the reconstruction of the tip of an acupuncture needle without/with the application of proposed method. Panel (c)/(d) is the reconstruction of a 100 µm circle from a calibration microscopy slide without/with the application of proposed method.

This method was reported in the following paper, attached at the end of this text:

"*Image enhancement and field of view enlargement in digital lensless holographic microscopy by multi-shot imaging*," J. Opt. Soc. Am. **A 40**, C150-C156 (2023) [27].

and was presented in the following conference:

"Improvement of the image reconstruction in digital lensless holographic microscopy by scanning of the sample plane," in Latin America Optics and Photonics (LAOP) Conference 2022, Technical Digest Series (Optica Publishing Group, 2022), paper W1D.2. [30]

The proceeding of this presentation is attached at the end of this text. Additionally, the improvement in the use of the OPU as a point source of spherical waves for DLHM was presented in the following conference, where was awarded with the third-place poster presentation. The submitted abstract is attached at the end of this text.

"Removal of perturbations from Optical-Pickup-Unit-based illumination for Digital Lensless Holographic Microscopy", XI Iberoamerican Optics Meeting / XIV Latin American Meeting on Optics, Lasers and Applications (RIAO-OPTILAS), San José, Costa Rica, 2023 [31]. Awarded with the **Third Place in Poster presentation.**

5. Recovery of sample information in presence of occlusions

In DLHM, as in any imaging technique, the presence of occlusions implies a distortion of the visualized images. During the hologram recording stage, in the case of two occluded objects, the spherical wavefront, produced by the point source, illuminates the first object closer to it producing a propagated diffracted pattern. This pattern then illuminates the second object in the line of sight which produces a second diffraction pattern that is recorded in the digital sensor. If the objects are structured samples, the recorded hologram with the superposed information of the occluded objects results in a distorted reconstruction for both objects, as was introduced in Section 1.2.3. In this chapter, the Multiview Correlation Method introduced in Chapter 2 is utilized to recover separately the information of occluded objects in DLHM. For simplicity, the analysis is done for two occluded samples, but as can be seen later in this chapter, the process can be applied to a further number of samples, if necessary.

Two samples located at z_1 and z_2 distances from the point source are used to prove the feasibility of the proposed method. The magnification for both samples are $M_1 = \frac{L}{z_1}$ and $M_2 = \frac{L}{z_1 + \Delta z}$ with $\Delta z = z_2 - z_1$, respectively. Therefore, the closest the sample to the point source, the larger the magnification of the diffraction pattern in the sensor plane, as is shown in Fig. 5-1 panel (a). If the real size of both samples is h, the patterns size at the recording plane are $H_1 = M_1 h$ and $H_2 = M_2 h$, respectively.

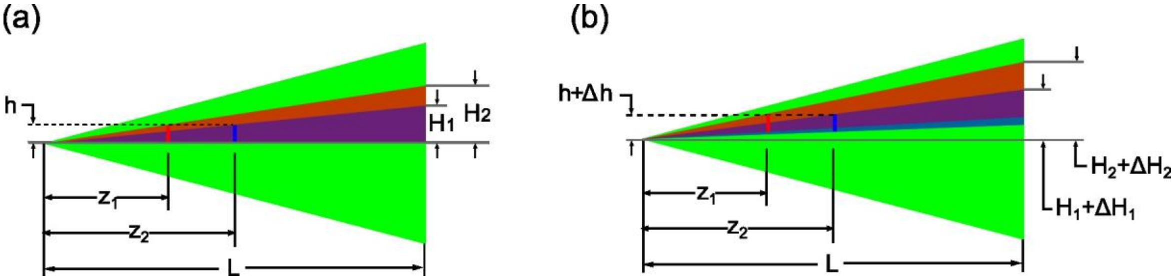

Fig. 5-1. Magnification at the sensor plane of two axially separated samples. Panels (a) and (b) show two lateral positions of the sample volume.

When the sample volume is lateral displaced a Δh distance, the magnified diffraction patterns of the different samples are proportionally displaced according to the corresponded magnification for each sample plane, resulting in different relative displacements $\Delta H_1 = M_1 \Delta h$ and $\Delta H_2 = M_2 h$, respectively. While $z_1 \neq z_2$, the displacements of the samples information over the sensor plane will be different. Comparing panels (a) and (b) of Fig. 5-1, it can be observed that the larger the distance z from the point source, the smaller the displacement of the diffraction pattern in the sensor plane.

According with the previous idea, if a set of in-line holograms recorded while a volume sample is displaced over its plane, different relative displacements for the diffraction pattern of the occluded samples can be observed. As a result, the information of each hologram in the set is rewritten following equation (2.2) as:

$$H_i(x,y) = I_{S_1}\left(x - \Delta \mathrm{x}_{S_{1,i}}, y - \Delta \mathrm{y}_{S_{1,i}}\right) I_{S_2}\left(x - \Delta \mathrm{x}_{S_{2,i}}, y - \Delta \mathrm{y}_{S_{2,i}}\right), \tag{5.1}$$

where $I_{S_1}(x,y)$ is the diffraction pattern of the occluded sample 1 displaced $(\Delta \mathrm{x}_{S_{1,i}}, \Delta \mathrm{y}_{S_{1,i}})$ over the recording plane. The same applies to $I_{S_2}(x,y)$ for sample 2.

To illustrate the application of the proposed method, the occluded USAF test target [50] and epithelial cheek cells presented in Section 1.2.3 were imaged using a DLHM setup. A 532 nm laser was focused on a 1 µm pinhole as the illumination source. The in-line holograms were recorded using a digital camera with (2048 x 2048) square pixels of 3.45 µm in side, located at $L = 18.4\,mm$ from the point source. Fig. 5-2 panel (a) shows the recorded fixed hologram used in the Multiview Correlation Method, and one of the recorded displaced holograms of the set, in panel (b), for the visualization of the USAF test target and the epithelial cheek cells. The template for the application of the Multiview Correlation Method is chosen for the sample from which the occlusion wants to be removed; for instance, if the USAF test target wants to be visualized, the purple rectangle should be chosen as the template of Fig. 5-2 (a), otherwise, if the sample of interest are the epithelial cheek cells the red rectangle should be the chosen template in the same figure.

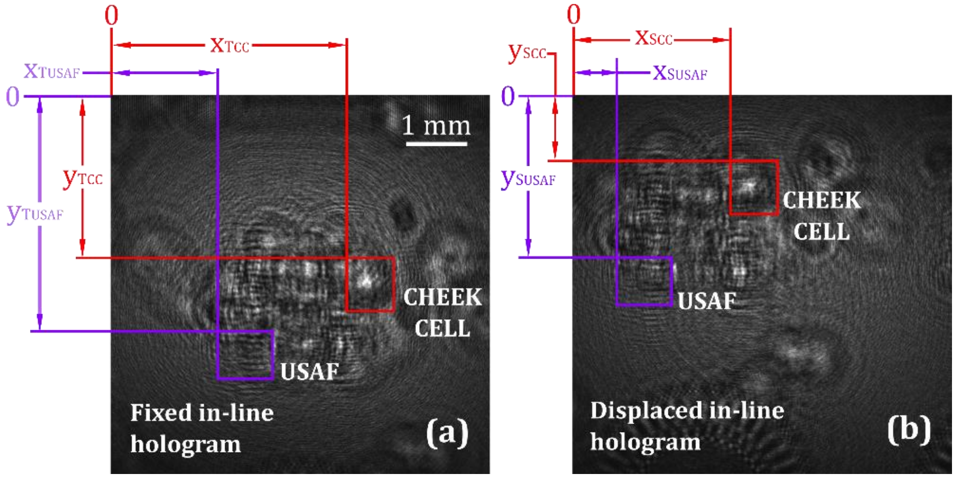

Fig. 5-2. The fixed recorded in-line hologram (a) and one displaced recorded in-line hologram (b) for the occlusion of a USAF test target and epithelial cheek cells.

As the relative displacements for both samples are different, a set of displaced in-line holograms can be recorded to apply the Multiview Correlation Method to remove the occlusions. If sample 1 was selected to eliminate the occlusion, its relative displacements, $\Delta \mathrm{x}_{S_{1,i}}$ and $\Delta y_{S_{1,i}}$, are determined to compose a new hologram by the coordinated addition of the in-line holograms of the set. In this composition, the information about sample 1 is conserved while the information about sample 2 is displaced, as is indicated in the composition equation as

$$H_{Comp_{S_1}}(x,y) = I_{S_1}(x,y) \sum_{i=1}^{N} I_{S_2}\left(x - \Delta \mathrm{x}_{S_{2,i}} + \Delta \mathrm{x}_{S_{1,i}}, y - \Delta \mathrm{y}_{S_{2,i}} + \Delta y_{S_{1,i}}\right) . \tag{5.2}$$

In this equation, sample 1 was selected to eliminate the occlusion, and given that $\Delta \mathrm{x}_{S_{1,i}} \neq \Delta \mathrm{x}_{S_{2,i}}$ and $\Delta \mathrm{y}_{S_{1,i}} \neq \Delta \mathrm{y}_{S_{2,i}}$, the displaced information about sample 2 turns into a homogeneous distribution preserving only the information of sample 1 and removing the occlusion. Equation (5.2) is therefore rewritten as

$$H_{Comp_{S_1}}(x,y) \approx I_{S_1}(x,y). \tag{5.3}$$

To remove the occlusions of sample 2, the same procedure should be followed to determine the relative displacements $\Delta \mathrm{x}_{S_{2,i}}$ and $\Delta y_{S_{2,i}}$ for the set of in-line holograms, and the composition equation is written as

$$H_{Comp_{S2}}(x,y) = I_{S_2}(x,y)\sum_{i=1}^{N} I_{S_1}\big(x - \Delta \mathrm{x}_{S_{1,i}} + \Delta \mathrm{x}_{S_{2,i}}, y - \Delta \mathrm{y}_{S_{1,i}} + \Delta y_{S_{2,i}}\big) \approx I_{S_2}(x,y). \tag{5.4}$$

The occlusion removed holograms for the USAF test target, and the epithelial cheek cells are shown in Fig. 5-3. The diffraction pattern of each sample is observed separately for each in-line hologram, anticipating that the occlusions are no longer be presented in their reconstructions.

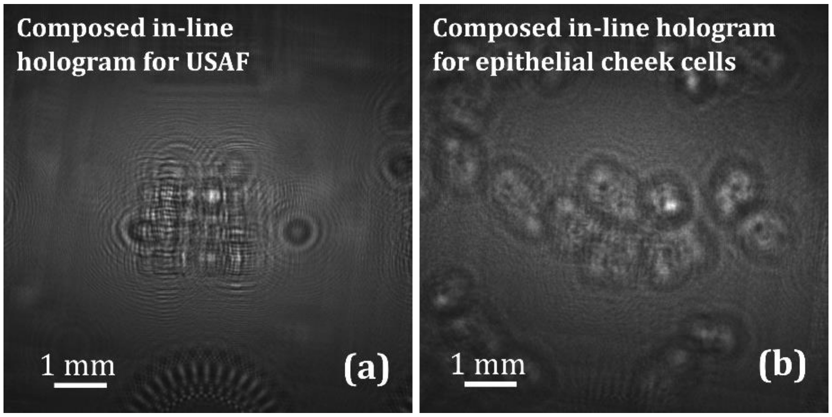

Fig. 5-3. The composite in-line holograms for the USAF test target (a) and the epithelial cheek cells (b) without the presence of occlusions.

In Fig. 5-4 panels (a) and (c), the reconstruction of the in-line and composite holograms from Fig. 5-2(a) and Fig. 5-3 (a) are shown, respectively. For both panels, the reconstruction distance was $z_1 = 1.70mm$, to get in focus the USAF test target image. In panel (a), the presence of the occlusion shows the out-of-focus information that ruins the information about the USAF test target, making it difficult to visualize clearly. In contrast, the application of the Multiview Correlation Method produces a clear reconstruction without the presence of information on out-of-focus planes, as is shown in panel (c). In Fig. 5-4 panels (b) and (d), the reconstruction of the in-line and composite holograms from Fig. 5-2(a) and Fig. 5-3 (b) are shown, respectively. For this case, the epithelial cheek cells were in focus at a distance $z_2 = 1.29mm$ from the point source. The comparison between those panels highlights the performance of the proposed method to remove the occlusion. The nuclei of the epithelial cheek cells are clearly visible in Fig. 5-4 (d) as purplish dots, and three of them are pointed out by arrows. This method also allows for an enlargement of the FOV by gathering information from multiple views of the sample volume, resulting in an enlargement of approximately 50% for this experiment, as is observed when the FOV of the reconstruction of the single hologram in panel (a)/(b) is compared with the reconstruction of the composite hologram in panel (c)/(d).

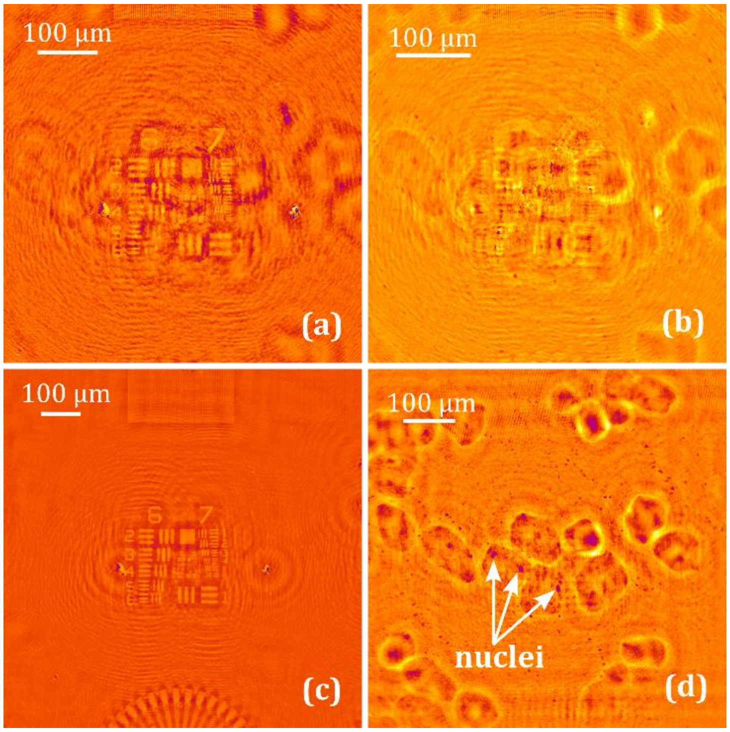

Fig. 5-4. Panel (a)/(b) shows the phase reconstruction of the fixed hologram for the USAF test target/epithelial cheek cells plane. In panel (c)/(d), the reconstruction of the composite hologram without occlusions is shown.

To validate the method for recovering the information of more than two samples axially separated, a 4 planes volume sample of epithelial cheek cells was imaged. The same pinhole-based setup and digital camera were utilized. The in-line DLHM holograms were recorded at *L*=18.4 mm, subtending a NA=0.19 for the optical setup. In Fig. 5-5 one single in-line hologram of the set is shown.

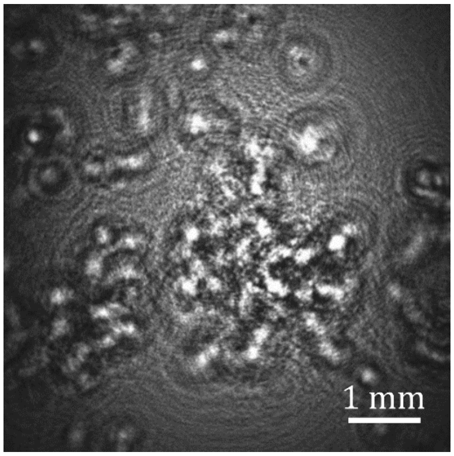

Fig. 5-5. Single in-line DLHM hologram of the occluded epithelial cheek cells volume sample.

Due to the existence of multiple sample planes, when the reconstruction procedure is performed, the information of the samples cannot be focused. The out-in-focus information generates a strong perturbation over the reconstructed complex-valued wavefield, limiting the identification of the focus planes. The composite holograms of the 4 sample planes, resulting from the application of the Multiview Correlation Method for removing the occlusions, are presented in Fig. 5-6 panels (a), (b), (c), and (d). In those composite holograms, the information of each plane of interest is preserved while the information of the out-of-focus planes is blurred. In panels (e), (f), (g) and (h) of Fig. 5-6, the reconstruction for the composite holograms at $z_1 = 1.84\, mm$, $z_2 = 2.09\, mm$, $z_3 = 2.62\, mm$, and $z_4 = 2.98\, mm$ to get in focus the 4 different planes of the epithelial cheek cells, are shown respectively. In those images, it is clear to identify the epithelial cheek cells of each axial separated plane at its corresponding z distance, while the out-of-focus information is blurred. Additionally, it is noted that the larger the axial distance between planes, the blurrier the information appears in the reconstructed plane. To illustrate the improvement of the method for the occlusion removal and the identification of the focus plane, the reconstructions of the in-line hologram presented in Fig. 5-5 for each determined z distance are shown in panels (i), (j), (k) and (l), respectively. It is clear that the occlusion generated by the presence of epithelial cheek cells in different axial locations made it impossible to identify the interest samples in the focus planes. However, the method enables removing the occlusions and proper visualizing the epithelial cheek cells in each plane.

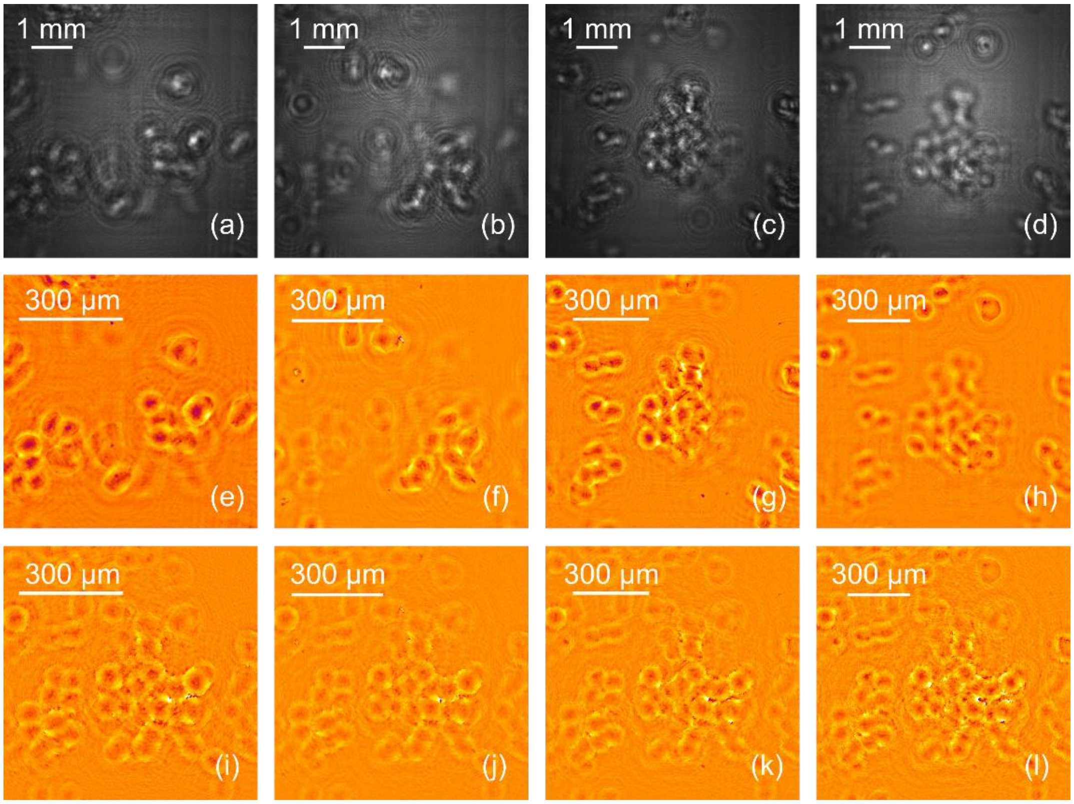

Fig. 5-6. Epithelial cheek cells multiplane (volumetric) sample. Panels (a), (b), (c), and (d) show the composite holograms of 4 sample planes of epithelial cheek cells. Panels (e), (f), (g), and (h) show the phase reconstructions of the mentioned composite holograms to get in-focus the four different planes of cells, respectively. Panels (i), (j), (k), and (l) show the reconstruction of the in-line hologram presented in Fig. 5-5 at the determined z distances for reconstructing the cells in panels (e), (f), (g), and (h), respectively.

The proposed method for recovery the information of occluded objects in DLHM was presented in the following conference and its submitted abstract is attached at the end of this text:

"Recovery of occluded objects in digital lensless holographic microscopy", XI Iberoamerican Optics Meeting / XIV Latin American Meeting on Optics, Lasers and Applications (RIAO-OPTILAS), San José, Costa Rica, 2023 [31]

6. Conclusions

6.1 Conclusions

The main results of obtained in this Master thesis in Engineering Physics can be summarized as follows:

A method for measuring the Numerical Aperture (NA) of Gaussian propagating light beams was reported. For the application of this method, two intensities distributions are recorded for two positions axially separate Δz; for each distribution, a bidimensional Gaussian fitting, using the Levenberg-Marquardt algorithm, is computed to determine their respective standard deviation of the Gaussian distributions. By taking the difference in the standard deviations and Δz, the NA can be calculated using a simple expression derived from Gaussian propagating beam theory. This method is useful for characterizing newly fabricated point sources, such as optical fiber cone tips or holographic point sources, as well as validating the NA of graded optical elements for it use in DLHM.

The feasibility of expanding the field of view (FOV) in DLHM without affecting the correct sampling of the diffracted information in the recorded hologram was presented. This method is based on the superposition of in-line holograms with different views of the sample to generate an expanded FOV in the reconstructed image. Moreover, giving the possibility of using low-cost sensors with a reduced size and reproducing the capabilities of a larger sensor without that implies a significant cost in the performance of the technique.

A method for correcting DLHM in-line holograms, called Multiview Correlation Method, was presented. In this method, the diffracted information of the sample is recorded in different positions of the FOV. A coordinated addition of the in-line holograms is performed considering the relative displacement between holograms, determined by the computation of the normalized cross-correlation (NCC). And finally, after normalizing, a corrected composite hologram is obtained.

To correct artifacts caused by the illumination source in DLHM, the Multiview Correlation Method was utilized. When artifacts are present in the illumination, they affect the information in the recorded hologram, resulting in perturbed information of the visualized sample. The application of the proposed method eliminates the presence of the artifacts by generating a composite hologram without the presence of illumination artifacts, producing a reconstruction free of those artifacts.

And finally, this method was utilized to recover the information of occluded objects in DLHM. As the diffraction pattern of the specimen in a volume sample is recorded in an in-line hologram, multiple objects in the same line of sight produce a merged coded information of those objects. Consequently, when an object is focused, the out-of-focus information distorts the reconstructed sample to the point that, in some cases is impossible to identify the focus plane of the sample. The Multiview Correlation Method was utilized to separate the information of the occluded objects in different holograms for each focus plane.

The proposed methods in this master's thesis present an improvement in the visualization of biosamples compared with the conventional DLHM visualization. Still, their application implies recording a set of displaced holograms, limiting their application to static samples. Additionally, the proposed compositions increase the computational cost and the processing time of the holograms comparted to the conventional method. Despite those limitations, the results presented in this master’s thesis evidence the achievement of the proposed objectives, overcoming different limitations evaluated in DLHM. The effectiveness of the former was confirmed by comparing the use of the proposed methods with conventional DLHM imaging. These methods were evaluated for the visualization of biosamples to show their feasibility in bioimaging applications.

6.2 Future work perspectives

The results achieved in this Master thesis in Engineering Physics have made significant progress in the overcoming limitations of DLHM for the visualization of biosamples, and also pointed towards the following research that can be further developed:

1. The method for measuring the NA could be integrated into a tool for the existing suit for ImageJ developed by the Optics and Opto-digital Processing Research Group (ODP).
2. The method for expanding the FOV could be incorporated into the existing DLHM plugin, and taking advantage of the capabilities that offer the Micromanager extension of ImageJ, the integration of motorized displacers for the sample stages should turn this method into a fully automated. This could be considered for a master’s thesis.
3. As was presented in chapter 3, the method for expanding the FOV invites to the development of a more cost-effective digital lensless holographic microscope than the currently reported in the literature.
4. For overcoming the limitation of visualizing only static samples for applying the Multiview Correlation Method, the use of an illumination array for recording the set of displaced holograms could be explored.
5. The Multiview Correlation Method, for its capabilities in correcting DLHM in-line holograms for illumination artifacts and occluded samples, should be integrated into a plugin for the existing suite of tools developed by the ODP.

A. Appendix: Attached manuscripts

Below are attached the two published manuscripts resulting from the presented master's thesis. They are presented in the format in which each was submitted to the corresponding journal, and ordered by their mention in the main text; namely:

Chapter 3: Improvements in the Numerical Aperture and FOV.

- "*Automatic method to measure the numerical aperture of a propagating Gaussian light beam*", Óptica Pura y Aplicada **55**, 1-8 (2022) [26].

Chapter 4: Overcoming the presence of illumination artifacts.

- "*Image enhancement and field of view enlargement in digital lensless holographic microscopy by multi-shot imaging*," J. Opt. Soc. Am. **A 40**, C150-C156 (2023) [27].

Additionally, the mentioned proceedings and submitted abstracts of the presented results in international conferences are also attached:

Chapter 3: Improvements in the Numerical Aperture and FOV.

- "*Método automático para la medición de la apertura numérica de haces de luz Gaussianos*", XVII Encuentro nacional de Óptica y XIII Conferencia Andina y del Caribe en Óptica y sus aplicaciones, Medellín Colombia, 2021 [28].
- *"Cost-effective digital lensless holographic microscope,"* in OSA Imaging and Applied Optics Congress (Online), Washington DC United States, 2021 [29].

Chapter 4: Overcoming the presence of illumination artifacts.

- *"Improvement of the image reconstruction in digital lensless holographic microscopy by scanning of the sample plane,"* in Latin America Optics and Photonics (LAOP) Conference 2022, Technical Digest Series (Optica Publishing Group, 2022), paper W1D.2. [30].
- *"Removal of perturbations from Optical-Pickup-Unit-based illumination for Digital Lensless Holographic Microscopy"*, XI Iberoamerican Optics Meeting / XIV Latin

American Meeting on Optics, Lasers and Applications (RIAO-OPTILAS), San José, Costa Rica, 2023 [31]. Awarded with Awarded with **Third Place in Poster presentation.**

Chapter 5: Recovery of sample information in presence of occlusions

- *“Recovery of occluded objects in digital lensless holographic microscopy”*, XI Iberoamerican Optics Meeting / XIV Latin American Meeting on Optics, Lasers and Applications (RIAO-OPTILAS), San José, Costa Rica, 2023 [32].

References

1. J. Garcia-Sucerquia, W. Xu, S. K. Jericho, P. Klages, M. H. Jericho, and H. J. Kreuzer, "Digital in-line holographic microscopy," Appl. Opt. **45**, 836 (2006).
2. H. Tobon-Maya, S. I. Zapata-Valencia, E. Zora-Guzmán, C. Buitrago-Duque, and J. Garcia-Sucerquia, "Open-source, cost-effective, portable, 3D-printed digital lensless holographic microscope," Appl. Opt. **60**, A205 (2021).
3. C. Trujillo, P. Piedrahita-Quintero, and J. Garcia-Sucerquia, "Digital lensless holographic microscopy: numerical simulation and reconstruction with ImageJ," Appl. Opt. **59**, 5788 (2020).
4. J. F. Restrepo and J. Garcia-Sucerquia, "Magnified reconstruction of digitally recorded holograms by Fresnel-Bluestein transform," Appl. Opt. **49**, 6430–6435 (2010).
5. C. Buitrago-Duque and J. Garcia-Sucerquia, "Non-approximated Rayleigh–Sommerfeld diffraction integral: advantages and disadvantages in the propagation of complex wave fields," Appl. Opt. **58**, G11 (2019).
6. P. Ferraro, A. Wax, and Z. Zalevsky, eds., *Coherent Light Microscopy*, Springer Series in Surface Sciences (Springer Berlin Heidelberg, 2011), Vol. 46.
7. W. Xu, M. H. Jericho, I. A. Meinertzhagen, and H. J. Kreuzer, "Digital in-line holography for biological applications," Proc. Natl. Acad. Sci. **98**, 11301–11305 (2002).
8. B. Ghosh and K. Agarwal, "Viewing life without labels under optical microscopes," Commun. Biol. **6**, (2023).
9. M. Cases, *The Introduction to Microbiology* (n.d.).
10. J. A. Picazo-Bueno, K. Trindade, M. Sanz, and V. Micó, "Design, Calibration, and Application of a Robust, Cost-Effective, and High-Resolution Lensless Holographic Microscope," Sensors **22**, 553 (2022).
11. M. Sanz, J. A. Picazo-Bueno, J. García, and V. Micó, "Improved quantitative

phase imaging in lensless microscopy by single-shot multi-wavelength illumination using a fast convergence algorithm," Opt. Express (2015).

12. H. Tobón-Maya, A. Gómez-Ramírez, C. Buitrago-Duque, and J. Garcia-Sucerquia, "Adapting a Blu-ray optical pickup unit as a point source for digital lensless holographic microscopy," Appl. Opt. **62**, D39 (2023).
13. C. Buitrago-Duque, B. Patiño-Jurado, and J. Garcia-Sucerquia, "Robust and compact digital Lensless Holographic microscope for Label-Free blood smear imaging," HardwareX **13**, e00408 (2023).
14. B. Patiño-Jurado, J. F. Botero-Cadavid, and J. Garcia-Sucerquia, "Cone-shaped optical fiber tip for cost-effective digital lensless holographic microscopy," Appl. Opt. **59**, 2969 (2020).
15. B. Patiño-Jurado, J. F. Botero-Cadavid, and J. Garcia-Sucerquia, "Step-Index Optical Fibers with 0.88 Numerical Aperture," J. Light. Technol. **37**, 3734–3739 (2019).
16. M. J. Lopera and C. Trujillo, "Holographic point source for digital lensless holographic microscopy," Opt. Lett. **47**, 2862 (2022).
17. A. A. Adeyemi and T. E. Darcie, "Expansion of field of view in digital in-line holography with a programmable point source," Appl. Opt. **48**, 3291–3301 (2009).
18. H. Tobon-Maya, C. Trujillo, and J. Garcia-Sucerquia, "Preprocessing in digital lensless holographic microscopy for intensity reconstructions with enhanced contrast," Appl. Opt. **60**, A215 (2021).
19. W. Xu, M. H. Jericho, H. J. Kreuzer, and I. A. Meinertzhagen, "Tracking particles in four dimensions with in-line holographic microscopy," Opt. Lett. **28**, 164 (2003).
20. A. Buades, B. Coll, and J.-M. Morel, "A Non-Local Algorithm for Image Denoising," in *2005 IEEE Computer Society Conference on Computer Vision and Pattern Recognition (CVPR'05)* (IEEE, n.d.), pp. 60–65.
21. K. Dabov, A. Foi, V. Katkovnik, and K. Egiazarian, *Image Denoising with Block-Matching and 3D Filtering* (2006).
22. J. J. Barton, "Photoelectron holography = holography + photoelectron diffraction," J. Electron Spectros. Relat. Phenomena **51**, 37–53 (1990).
23. S. K. K. Jericho, J. Garcia-Sucerquia, W. Xu, M. H. H. Jericho, and H. J. J. Kreuzer, "Submersible digital in-line holographic microscope," Rev. Sci. Instrum. **77**, 43706–43710 (2006).

24. S. K. Jericho, P. Klages, J. Nadeau, E. M. Dumas, M. H. Jericho, and H. J. Kreuzer, "In-line digital holographic microscopy for terrestrial and exobiological research," Planet. Space Sci. **58**, 701–705 (2010).
25. J. S. Underkoffler, "Occlusion Processing and Smooth Surface Shading for Fully Computed Synthetic Holography," Pract. Hologr. XI Hologr. Mater. III **3011**, 19–30 (1997).
26. S. I. Zapata-Valencia, H. Tobon-Maya, and J. García-Sucerquia, "Automatic method to measure the numerical aperture of a propagating Gaussian light beam," Opt. Pura y Apl. **55**, 1–8 (2022).
27. S. I. Zapata-Valencia, H. Tobon-Maya, and J. Garcia-Sucerquia, "Image enhancement and field of view enlargement in digital lensless holographic microscopy by multi-shot imaging," J. Opt. Soc. Am. A **40**, C150 (2023).
28. S. I. Zapata-Valencia, H. Tobon-Maya, and J. Garcia-Sucerquia, *Método Automático Para La Medición de La Apertura Numérica de Haces de Luz Gaussianos.* (2021).
29. S. I. Zapata-Valencia, H. Tobon-Maya, C. Buitrago-Duque, and J. Garcia-Sucerquia, "Cost-effective digital lensless holographic microscope," in *OSA Imaging and Applied Optics Congress 2021 (3D, COSI, DH, ISA, PcAOP)* (Optica Publishing Group, 2021), Vol. 60, p. DW4C.3.
30. S. I. Zapata-Valencia and J. Garcia-Sucerquia, "Improvement of the image reconstruction in digital lensless holographic microscopy by scanning of the sample plane," in *Latin America Optics and Photonics (LAOP) Conference 2022* (Optica Publishing Group, 2022), p. W1D.2.
31. S. I. Zapata-Valencia, H. Tobon-Maya, and J. Garcia-Sucerquia, *Removal of Perturbations from Optical-Pickup-Unit-Based Illumination for Digital Lensless Holographic Microscopy* (2023).
32. S. I. Zapata-Valencia, H. Tobon-Maya, and J. Garcia-Sucerquia, *Recovery of Occluded Objects in Digital Lensless Holographic* (2023).
33. D. Gabor, "A new microscopic principle," Nature **161**, 777–778 (1948).
34. J. F. Restrepo and J. Garcia-Sucerquia, "Diffraction-based modeling of high-numerical-aperture in-line lensless holograms," Appl. Opt. **50**, 1745 (2011).
35. U. Schnars and W. P. O. Jueptner, "Digital recording and numerical reconstruction of holograms," Meas. Sci. Technol. **13**, 85–101 (2002).

36. L. Repetto, F. Pellistri, E. Piano, and C. Pontiggia, "Gabor’s hologram in a modern perspective," Am. J. Phys. **72**, 964–967 (2004).

37. J. W. Goodman, *Introduction to Fourier Optics*, 3rd Editio (Roberst & Company Publishers, 2005).

38. C. C. Chernecky and B. J. Berger, *Laboratory Tests and Diagnostic Procedures*, 6th ed. (Elsevier Health Sciences, 2013).

39. J. Garcia-Sucerquia, "Color lensless digital holographic microscopy with micrometer resolution," Opt. Lett. **37**, 1724 (2012).

40. M. J. Lopera and C. Trujillo, "Linear diattenuation imaging of biological samples with digital lensless holographic microscopy," Appl. Opt. **61**, B77 (2022).

41. E. Serabyn, K. Liewer, C. Lindensmith, K. Wallace, and J. Nadeau, "Compact, lensless digital holographic microscope for remote microbiology," Opt. Express **24**, 28540–28548 (2016).

42. M. Sanz, M. Trusiak, J. García, and V. Micó, "Variable zoom digital in-line holographic microscopy," Opt. Lasers Eng. **127**, (2020).

43. N. I. Lewis, X. Wenbo, S. K. Jericho, H. J. Kreuzer, M. H. Jericho, and A. D. Cembella, "Swimming speed of three species of Alexandrium (Dinophyceae) as determined by digital in-line holography," Phycologia **45**, 61–70 (2006).

44. E. Hecht, *Optics*, 4th ed. (Addison Wesley Publishing Company, 2002).

45. J. W. Goodman, *Statistical Optics*, 1st ed. (Wiley, 2000).

46. S. Grare, "Compact, low-cost Blu-Ray pickup-based digital holographic microscope," Opt. Lasers Eng. **160**, 107272 (2023).

47. H.-Y. Chung, W.-C. Kuo, Y.-H. Cheng, C.-H. Yu, S.-H. Chia, C.-Y. Lin, J.-S. Chen, H.-J. Tsai, A. B. Fedotov, A. A. Ivanov, A. M. Zheltikov, and C.-K. Sun, "Blu-ray disk lens as the objective of a miniaturized two-photon fluorescence microscope," Opt. Express **21**, 31604 (2013).

48. E. E. Te Hwu and A. Boisen, "Hacking CD/DVD/Blu-ray for Biosensing," ACS Sensors (2018).

49. Blu-ray Disc Association, "White Paper Blu-Ray Disc (TM) format -physical format specifications for BD-ROM," (2010).

50. Applied Image Inc, "USAF 1951 Chart - Standard Layout," (n.d.).

51. V. Bianco, P. Memmolo, P. Carcagnì, F. Merola, M. Paturzo, C. Distante, and P. Ferraro, "Microplastic Identification via Holographic Imaging and Machine

Learning," Adv. Intell. Syst. **2**, 1900153 (2020).

52. Y. Zhu, C. Hang Yeung, and E. Y. Lam, "Digital holographic imaging and classification of microplastics using deep transfer learning," Appl. Opt. **60**, A38–A47 (2021).
53. J. Maycock, C. P. McElhinney, B. M. Hennelly, T. J. Naughton, J. B. McDonald, and B. Javidi, "Reconstruction of partially occluded objects encoded in three-dimensional scenes by using digital holograms," Appl. Opt. **45**, 2975–2985 (2006).
54. B. Javidi, R. Ponce-Díaz, and S.-H. Hong, "Three-dimensional recognition of occluded objects by using computational integral imaging," Opt. Lett. **31**, 1106 (2006).
55. P. Hariharan, *Optical Holography: Principles, Techniques, and Applications*, 2nd ed. (Cambridge University Press, 1996).
56. H. F. Durrant-Whyte, "Sensor Models and Multisensor Integration," Int. J. Rob. Res. **7**, 97–113 (1988).
57. J. P. Lewis, "Fast Template Matching," in *Vision Interface 95* (Canadian Image Processing and Pattern Recognition Society, Quebec City, Canada, May 15-19, 1995), pp. 120–123.
58. J. Garcia-Sucerquia, D. Alvarez-Palacio, and J. Kreuzer, "Digital In-line Holographic Microscopy of Colloidal Systems of Microspheres," in *Adaptive Optics: Analysis and Methods/Computational Optical Sensing and Imaging/Information Photonics/Signal Recovery and Synthesis Topical Meetings*, OSA, ed. (OSA, 2007).
59. A. E. Siegman, *Lasers*, 1st ed. (University Science Books, 1986).
60. K. Levenberg, "A method for the solution of certain non-linear problems in least squares," Q. Appl. Math. **2**, 164–168 (1944).
61. D. Gabor, "Microscopy by reconstructed wave-fronts," in *Proceedings of the Royal Society of London. Series A. Mathematical and Physical Sciences* (1949), pp. 454–487.
62. R. A. Frazor and W. S. Geisler, "Local luminance and contrast in natural images," Vision Res. **46**, 1585–1598 (2006).